PHYSICAL REVIEW D **87,** 114513 (2013)

Determination of the $\Delta(1232)$ axial and pseudoscalar form factors from lattice QCD

Constantia Alexandrou*
Department of Physics, University of Cyprus, P.O. Box 20537, 1678 Nicosia, Cyprus and The Cyprus Institute, P.O. Box 27546, 1645 Nicosia, Cyprus

Eric B. Gregory
Bergische Universität Wuppertal, Gaußstraße 20, D-42119 Wuppertal, Germany

Tomasz Korzec
Institut für Physik, Humboldt Universität zu Berlin, Newtonstrasse 15, 12489 Berlin, Germany

Giannis Koutsou
Cyprus Institute, CaSToRC, 20 Kavafi Street, Nicosia 2121, Cyprus

John W. Negele
Laboratory for Nuclear Science and Department of Physics, Center for Theoretical Physics, Massachusetts Institute of Technology, Cambridge, Massachusetts 02139, USA

Toru Sato
Department of Physics, Osaka University, Osaka 560-0043, Japan

Antonios Tsapalis
Hellenic Naval Academy, Hatzikyriakou Avenue, Pireaus 18539, Greece and Department of Physics, National Technical University of Athens, Zografou Campus 15780 Athens, Greece
(Received 21 April 2013; published 26 June 2013)

We present a lattice QCD calculation of the $\Delta(1232)$ matrix elements of the axial-vector and pseudoscalar currents. The decomposition of these matrix elements into the appropriate Lorentz invariant form factors is carried out, and the techniques to calculate the form factors are developed and tested using quenched configurations. Results are obtained for $2 + 1$ domain wall fermions and within a hybrid scheme with domain wall valence and staggered sea quarks. Two Goldberger-Treiman–type relations connecting the axial to the pseudoscalar effective couplings are derived. These and further relations based on the pion-pole dominance hypothesis are examined using the lattice QCD results, finding support for their validity. Using lattice QCD results on the axial charges of the nucleon and the Δ, as well as the nucleon-to-Δ transition coupling constant, we perform a combined chiral fit to all three quantities and study their pion mass dependence as the chiral limit is approached.

DOI: 10.1103/PhysRevD.87.114513 PACS numbers: 11.15.Ha, 12.38.Aw, 12.38.Gc, 14.20.Gk

I. INTRODUCTION

Great progress has been made in lattice QCD studies of hadron spectroscopy and structure, and lattice QCD results are beginning to provide input to phenomenology and experiment. Simulations with dynamical quarks near and at the physical pion mass [1–4] have been shown to produce the observed low-lying hadron spectrum [2,5,6], and $\pi^+ - \pi^+$ scattering lengths have been calculated to good accuracy [7–10].

Whereas producing experimentally measured quantities from first principles provides a powerful validation of the lattice QCD methodology, calculating quantities that are difficult to extract or have an impact in probing physics beyond the standard model is a much more challenging prospect. Studying the structure of the Δ resonance is an example of the input lattice QCD can provide to phenomenology that cannot be directly extracted from experiments. This is because the Δ decays strongly with a lifetime of $\sim 10^{-23}$ seconds [11,12] and resists experimental probing. Measurements of the Δ^+ magnetic moment exist albeit with a large experimental uncertainty. The Δ, having width $\Gamma \sim 118$ MeV and lying close to the πN threshold, plays an important role in chiral expansions. In heavy baryon chiral perturbation theory, it has been included as an explicit degree of freedom [13–16], where it is argued that it improves chiral expansions applied in the description of lattice QCD results such as the nucleon axial charge [17]. Chiral Langragians with Δ degrees of freedom involve additional coupling constants that are difficult to measure. Therefore, one either treats them as free

*Corresponding author.
alexand@ucy.ac.cy

parameters to be fitted along other parameters using lattice QCD results [13,18] and data extracted from partial-wave analysis of scattering measurements [15,16] or estimates them based on phenomenology and symmetries. For example, one can relate the nucleon axial charge g_A, which is well measured, to the Δ axial charge, in the large-N_c limit [19] or using $SU(4)$ symmetry [20]. The Goldberger-Treiman (GT) relation is then used to get the effective $\pi\Delta\Delta$ coupling. Another framework to extract the $\pi\Delta\Delta$ coupling is via sum rules [21].

Lattice QCD provides a nice framework to study the Δ properties and calculate the Δ coupling constants. In some of our recent work, we developed the formalism to study the $N-\Delta$ transition form factors within lattice QCD [22,23], as well as the Δ electromagnetic form factors [24]. The quadrupole electromagnetic form factor, extracted for the first time, provided input for the deformation of the Δ showing that in the infinite momentum frame the Δ is prolate [25].

In this work, we present a detailed study of the axial-vector and pseudoscalar form factors of the Δ. The theoretical framework and a subset of the results were given in Ref. [26]. Here we discuss in detail the lattice techniques developed and used for the extraction of these form factors. In addition, we present an extended analysis of the momentum dependence of all the form factors using an additional ensemble of dynamical domain wall fermions. We also include a study of the pion-pole dominance predictions and compare them to our lattice QCD results.

The outline of the paper is as follows. In Sec. II we present the decomposition of the Δ matrix elements of the axial-vector and pseudoscalar currents. In Sec. III we explain our lattice techniques and discuss the ensembles used for the calculation. In Sec. IV we present the lattice results on all form factors and examine several relations among them and their phenomenological consequences. In Sec. V we perform a combined chiral fit using our results on the nucleon axial charge g_A [27], the Δ axial charge $G_{\Delta\Delta}$ calculated in this work, and the dominant axial $N-\Delta$ transition form factor, C_5^A, calculated in previous work on the same sets of lattices [23]. Finally, in Sec. VI we give a summary and conclusions. Technical details and our values on the form factors are presented in the appendices.

II. AXIAL AND PSEUDOSCALAR MATRIX ELEMENT OF THE Δ

Lorentz invariance and spin-parity rules determine the decomposition of the Δ^+ matrix element of the isovector axial-vector current in terms of four invariant functions of the momentum transfer squared, $q^2=(p_f-p_i)^2$:

$$\langle\Delta^+(p_f,s_f)|A^\mu(0)|\Delta^+(p_i,s_i)\rangle=\bar{u}^\Delta_\sigma(p_f,s_f)[\mathcal{O}^{\mu\mathrm{A}}]^{\sigma\tau}u^\Delta_\tau(p_i,s_i)$$
$$[\mathcal{O}^{\mu\mathrm{A}}]^{\sigma\tau}=-\frac{1}{2}\left[g^{\sigma\tau}\left(g_1(q^2)\gamma^\mu\gamma^5+g_3(q^2)\frac{q^\mu}{2M_\Delta}\gamma^5\right)+\frac{q^\sigma q^\tau}{4M_\Delta^2}\left(h_1(q^2)\gamma^\mu\gamma^5+h_3(q^2)\frac{q^\mu}{2M_\Delta}\gamma^5\right)\right], \tag{1}$$

where $p_i(s_i)$ denotes the initial momentum (spin) of the Δ and $p_f(s_f)$ the final momentum (spin). The flavor-isovector axial-vector current operator is defined as

$$A^\mu(x)=\bar{\psi}(x)\gamma^\mu\gamma_5\frac{\tau^3}{2}\psi(x), \tag{2}$$

where τ^3 denotes the Pauli matrix acting in flavor space and $\psi(x)$ is the isospin quark doublet. The four axial form factors, g_1, g_3, h_1, and h_3 as defined in Eq. (1) are grouped into the familiar structure of the nucleon axial-vector vertex.

In the description of spin-3/2 energy-momentum eigenstates, classical solutions of the Rarita-Schwinger equation play a central role. Each component of a vector-spinor u_σ, with σ a Lorentz four-vector index solves the free Dirac equation

$$[\not{p}-M_\Delta]u^\Delta_\sigma(p,s)=0. \tag{3}$$

Implementing additionally the constraint equations,

$$p^\sigma u^\Delta_\sigma(p,s)=0\quad\text{and}\quad\gamma^\sigma u^\Delta_\sigma(p,s)=0, \tag{4}$$

the unphysical components are eliminated, and the remaining 8 degrees of freedom describe a spin-3/2 (anti)particle. Rarita-Schwinger spinors satisfy the spin sum relation:

$$\Lambda_{\sigma\tau}\equiv\sum_{s=-3/2}^{3/2}u^\Delta_\sigma(p,s)\bar{u}^\Delta_\tau(p,s)$$
$$=-\frac{\not{p}+M_\Delta}{2M_\Delta}\left(g_{\sigma\tau}-\frac{\gamma_\sigma\gamma_\tau}{3}-\frac{2p_\sigma p_\tau}{3M_\Delta^2}+\frac{p_\sigma\gamma_\tau-p_\tau\gamma_\sigma}{3M_\Delta}\right), \tag{5}$$

where the normalization $\bar{u}^{\Delta\sigma}u^\Delta_\sigma=-1$ is assumed.

The zero momentum transfer limit of Eq. (1) defines the axial charge, $G_{\Delta\Delta}$, of the Δ multiplet. Reference [28] normalizes the axial charge via

$$\langle\Delta^{++}|A^3_\mu|\Delta^{++}\rangle-\langle\Delta^-|A^3_\mu|\Delta^-\rangle=G_{\Delta\Delta}\mathcal{M}_\mu, \tag{6}$$

where $\mathcal{M}_\mu$ encodes the spin structure of the forward matrix element

$$\mathcal{M}_\mu=\bar{u}^{\Delta\sigma}(p)\gamma_\mu\gamma_5u^\Delta_\sigma(p). \tag{7}$$

Following the above normalization, we establish via Eq. (1)

$$G_{\Delta\Delta}=-3g_1(0). \tag{8}$$

We note that while the Lorentz decomposition of the axial current is naturally expressed via g_1, g_3, h_1, and h_3 as in Eq. (1), a decomposition in terms of multipoles is possible as, for example, in the case of the Δ electromagnetic transition [24]. Such a representation is more easily expressed in the Breit frame. This decomposition is performed in Appendix A in terms of four multipoles, L_1, L_3, E_1, and E_3, and their relation to the form factors g_1, g_3, h_1, and h_3 is given.

The Δ^+ matrix element of the pseudoscalar density operator

$$P(x) = \bar{\psi}(x)\gamma_5 \frac{\tau^3}{2}\psi(x) \tag{9}$$

is decomposed in terms of two Lorentz invariant form factors, denoted by $\tilde{g}(q^2)$ and $\tilde{h}(q^2)$:

$$\langle\Delta^+(p_f,s_f)|P(0)|\Delta^+(p_i,s_i)\rangle = \bar{u}^\Delta_\sigma(p_f,s_f)[\mathcal{O}^{\mathrm{P}}]^{\sigma\tau}u^\Delta_\tau(p_i,s_i),$$
$$[\mathcal{O}^{\mathrm{PS}}]^{\sigma\tau} = -\frac{1}{2}\left[g^{\sigma\tau}(\tilde{g}\gamma^5) + \frac{q^\sigma q^\tau}{4M_\Delta^2}(\tilde{h}\gamma^5)\right]. \tag{10}$$

While $\tilde{g}(q^2)$ and $\tilde{h}(q^2)$ are the directly computable form factors from the three-point pseudoscalar correlator, they can be related to the phenomenologically more interesting pion-Δ vertex using the partially conserved axial current hypothesis (PCAC). Using the PCAC on the hadronic level one can write

$$\partial^\mu A^a_\mu = f_\pi m_\pi^2 \pi^a, \tag{11}$$

with π^a denoting the isotriplet pion field operator. In the SU(2) symmetric limit of QCD with m_q denoting the up/down mass, the pseudoscalar density is related to the divergence of the axial-vector current through the axial Ward-Takahashi identity (AWI)

$$\partial^\mu A^a_\mu = 2m_q P^a = f_\pi m_\pi^2 \pi^a, \tag{12}$$

with operators now defined as quark bilinears. Using the relations of Eqs. (11) and (12), we identify the physically relevant pion-Δ-Δ from factor $G_{\pi\Delta\Delta}(q^2)$, which at $q^2 = 0$ gives the $\pi\Delta\Delta$ coupling, as well as a second form factor $H_{\pi\Delta\Delta}(q^2)$, by rewriting the pseudoscalar matrix element as

$$2m_q\langle\Delta^+(p_f,s_f)|P(0)|\Delta^+(p_i,s_i)\rangle$$
$$\equiv \frac{f_\pi m_\pi^2}{(q^2-m_\pi^2)}\times\bar{u}^\Delta_\sigma\left[g^{\sigma\tau}G_{\pi\Delta\Delta}(q^2) + \frac{q^\sigma q^\tau}{4M_\Delta^2}H_{\pi\Delta\Delta}(q^2)\right]\gamma^5 u^\Delta_\tau, \tag{13}$$

where we effectively make the identification

$$G_{\pi\Delta\Delta}(q^2) \equiv \frac{m_q(m_\pi^2 - q^2)}{f_\pi m_\pi^2}\tilde{g}(q^2) \tag{14}$$

$$H_{\pi\Delta\Delta}(q^2) \equiv \frac{m_q(m_\pi^2 - q^2)}{f_\pi m_\pi^2}\tilde{h}(q^2). \tag{15}$$

At zero momentum transfer $q^2 = 0$, only $G_{\pi\Delta\Delta}$ can be extracted. This coupling is analogous to the known $\pi - N$ pseudoscalar coupling constant $G_{\pi NN}$ defined for the nucleon. For the discussion presented in the next section, it is useful to recall the definition of the corresponding quantities in the nucleon sector [22]. For the matrix elements of the axial-vector current, we have

$$\langle N(p_f,s_f)|A^3_\mu|N(p_i,s_i)\rangle$$
$$= i\frac{1}{2}\bar{u}_N\left[G_A(q^2)\gamma_\mu\gamma_5 + \frac{q_\mu\gamma_5}{2m_N}G_p(q^2)\right]u_N, \tag{16}$$

and for the pseudoscalar density

$$2m_q\langle N(p_f,s_f)|P^3|N(p_i,s_i)\rangle$$
$$= \frac{f_\pi m_\pi^2}{(q^2-m_\pi^2)}\times\bar{u}_N[G_{\pi NN}(q^2)]i\gamma^5 u_N. \tag{17}$$

Note that we have dropped for simplicity an overall kinematical factor arising from the normalization of lattice states, since it is of no relevance for our discussion here.

A. Goldberger-Treiman relations

In this section we apply the PCAC to derive GT relations for the Δ. We recall that the PCAC has been shown to apply satisfactorily in the nucleon case leading to the GT relation. This can be derived from Eqs. (16) and (17) related by AWI and taking $q^2 = 0$ to obtain $G_{\pi NN}$ in terms of the nucleon axial charge via the relation

$$f_\pi G_{\pi NN}(0) = m_N G_A(0). \tag{18}$$

Assuming $G_{\pi NN}$ varies smoothly with q^2 so that $G_{\pi NN}(0) \sim G_{\pi NN}(m_\pi^2) \equiv g_{\pi NN}$, then the GT relates the physical coupling constant $g_{\pi NN}$ with the nucleon axial charge g_A. At the chiral limit, using $\partial_\mu A_\mu = 0$ one derives that $G_p(q^2) = -\frac{4m_N^2}{q^2}G_A(q^2)$. Therefore, $g_{\pi NN}$ measures the chiral symmetry breaking. The PCAC dictates that the form factor $G_p(q^2)$ has a pion pole given by $G_p(q^2) = \frac{4m_N f_\pi}{m_\pi^2 - q^2}G_{\pi NN}(q^2)$. The validity of the GT relation and the momentum dependence of $G_p(q^2)$ in the nucleon case has been studied in Ref. [22]. Similarly, a nondiagonal GT relation, applicable to the axial N-to-Δ transition is formulated and relates the axial $N\Delta$ coupling c_A to the $\pi N\Delta$ effective coupling. Lattice calculations examined the validity of the nondiagonal GT relation using the same ensembles as in this work [23].

One can similarly derive GT relations for the Δ by taking the matrix elements of the AWI with Δ states, $\langle\Delta|\partial_\mu A^\mu|\Delta\rangle = 2m_q\langle\Delta|P|\Delta\rangle$. Taking the dot product of q_μ with the matrix element of the axial-vector current given in Eq. (1), we obtain

$$m_\Delta\left[g^{\sigma\tau}(g_1 - \tau g_3) + \frac{q^\sigma q^\tau}{4M_\Delta^2}(h_1 - \tau h_3)\right]$$
$$= \frac{f_\pi m_\pi^2}{(m_\pi^2 - q^2)}\left[g^{\sigma\tau}G_{\pi\Delta\Delta} + \frac{q^\sigma q^\tau}{4M_\Delta^2}H_{\pi\Delta\Delta}\right], \tag{19}$$

where $\tau = -q^2/(2M_\Delta)^2$. By considering $\sigma \neq \tau$ in Eq. (19), we derive the relation

$$m_\Delta(h_1 - \tau h_3) = \frac{f_\pi m_\pi^2 H_{\pi\Delta\Delta}(q^2)}{m_\pi^2 - q^2}, \quad (20)$$

which implies that

$$M_\Delta(g_1 - \tau g_3) = \frac{f_\pi m_\pi^2 G_{\pi\Delta\Delta}(q^2)}{m_\pi^2 - q^2}. \quad (21)$$

One possible linear combination of Eqs. (20) and (21) can be obtained by taking the dot product of Eq. (19) with q_τ leading to

$$M_\Delta[(g_1 - \tau g_3) - \tau(h_1 - \tau h_3)] = \frac{f_\pi m_\pi^2}{m_\pi^2 - q^2}[G_{\pi\Delta\Delta} - \tau H_{\pi\Delta\Delta}], \quad (22)$$

which can be considered as a generalized GT-type relation connecting all the six form factors. At $q^2 = 0$ and assuming all terms in Eq. (22) are finite, we obtain

$$f_\pi G_{\pi\Delta\Delta}(0) = m_\Delta g_1(0). \quad (23)$$

If $G_{\pi\Delta\Delta}$ is a continuous slow varying function of q^2 as $q^2 \to 0$, then $G_{\pi\Delta\Delta}(m_\pi^2) \sim G_{\pi\Delta\Delta}(0)$, and we thus derive a GT relation for the Δ analogous to the one for the nucleon case.

Using Eq. (20) and setting $q^2 = 0$, we obtain a second GT relation:

$$f_\pi H_{\pi\Delta\Delta}(0) = m_\Delta h_1(0). \quad (24)$$

If one invokes pion-pole dominance and notes that g_1 and $G_{\pi\Delta\Delta}$ are both finite at the origin, it follows from Eqs. (21) and (20) that, as $q^2 \to m_\pi^2$, g_3 and h_3 must have a pole at $q^2 = m_\pi^2$. We thus arrive at the relations

$$g_1 = \frac{f_\pi}{M_\Delta} G_{\pi\Delta\Delta}, \qquad g_3 = \frac{4 f_\pi M_\Delta}{m_\pi^2 - q^2} G_{\pi\Delta\Delta} \quad (25)$$

and

$$h_1 = \frac{f_\pi}{M_\Delta} H_{\pi\Delta\Delta}, \qquad h_3 = \frac{4 f_\pi M_\Delta}{m_\pi^2 - q^2} H_{\pi\Delta\Delta}. \quad (26)$$

It is thus interesting to note how the spin-3/2 nature of the Δ state combined with the PCAC leads to a pair of Goldberger-Treiman relations, given by Eqs. (23) and (24). Let us examine further these relations at the chiral limit. From Eq. (22) we find that

$$h_1 - \tau h_3 = \frac{g_1 - \tau g_3}{\tau}, \quad (27)$$

which means that in the limit $q^2 \to 0$, the leading behavior of $h_1 \sim 1/q^2$, $h_3 \sim 1/(q^2)^2$ via Eq. (20) and $H_{\pi\Delta\Delta} \sim 1/q^2$ via Eq. (26). Therefore, the second GT-type relation given in Eq. (24) cannot be extrapolated to a physical pion mass since the assumption that h_1 and $H_{\pi\Delta\Delta}$ are slowly varying functions of q^2 no longer holds. However, since they both display a pion-pole behavior, one can factor it out on both sides, and thus the ratio $h_1/H_{\pi\Delta\Delta}$ can be extrapolated to the physical pion. In this sense, this constitutes a second GT relation.

III. LATTICE EVALUATION

A. Euclidean correlators and form factors

Standard techniques are employed on the Euclidean space-time lattice for the evaluation of hadronic form factors. The following two-point and three-point functions are required:

$$\begin{aligned} G_{\sigma\tau}(\Gamma^\nu, \vec{p}, t_f) &= \sum_{\vec{x}_f} e^{-i\vec{x}_f\cdot\vec{p}} \Gamma^\nu_{\alpha'\alpha} \langle \chi_{\sigma\alpha}(t_f, \vec{x}_f) \bar{\chi}_{\tau\alpha'}(0, \vec{0})\rangle \\ G^{\mathrm{A}}_{\sigma\mu\tau}(\Gamma^\nu, \vec{q}, t; t_f) &= \sum_{\vec{x}, \vec{x}_f} e^{+i\vec{x}\cdot\vec{q}} \Gamma^\nu_{\alpha'\alpha} \langle \chi_{\sigma\alpha}(t_f, \vec{x}_f) A_\mu(t, \vec{x}) \bar{\chi}_{\tau\alpha'}(0, \vec{0})\rangle \\ G^{\mathrm{PS}}_{\sigma\tau}(\Gamma^\nu, \vec{q}, t; t_f) &= \sum_{\vec{x}, \vec{x}_f} e^{+i\vec{x}\cdot\vec{q}} \Gamma^\nu_{\alpha'\alpha} \langle \chi_{\sigma\alpha}(t_f, \vec{x}_f) P(t, \vec{x}) \bar{\chi}_{\tau\alpha'}(0, \vec{0})\rangle, \end{aligned} \quad (28)$$

where $P(t, \vec{x})$ and $A_\mu(t, \vec{x})$ are the lattice pseudoscalar or axial current insertions, and χ is the standard lattice interpolating field with overlap with the Δ^+ quantum numbers,

$$\chi^{\Delta^+}_{\sigma\alpha}(x) = \frac{1}{\sqrt{3}} \epsilon^{abc}[2(\mathbf{u}^{a\top}(x) C\gamma_\sigma \mathbf{d}^b(x))\mathbf{u}^c_\alpha(x) + (\mathbf{u}^{a\top}(x) C\gamma_\sigma \mathbf{u}^b(x))\mathbf{d}^c_\alpha(x)]. \quad (29)$$

The overlap of χ with the spin-3/2 Δ^+ is

$$\begin{aligned} \langle \Omega | \chi_{\sigma\alpha}(0) | \Delta(p, s)\rangle &= Z u^\Delta_{\sigma\alpha}(p, s), \\ \langle \Delta(p, s) | \bar{\chi}_{\sigma\alpha}(0) | \Omega\rangle &= Z^* \bar{u}^\Delta_{\sigma\alpha}(p, s). \end{aligned} \quad (30)$$

We will use the following Γ matrices, which project onto positive parity for zero momentum, for our calculation:

$$\Gamma^4 = \frac{1}{4}(\mathbf{1} + \gamma^4), \qquad \Gamma^k = \frac{i}{4}(\mathbf{1} + \gamma^4)\gamma_5\gamma_k, \quad k = 1, 2, 3. \quad (31)$$

The Fourier transforms in Eq. (28) enforce a static Δ sink at the time slice t_f and a momentum transfer $\vec{q} = -\vec{p}$ injected via the operator insertion at an intermediate time slice t.

We insert into these correlators complete sets of hadronic energy momentum eigenstates:

$$\sum_{n,p,\xi} \frac{M_n}{V E_{n(p)}} |n(p,\xi)\rangle\langle n(p,\xi)| = \mathbf{1}, \tag{32}$$

where with ξ we denote collectively all quantum numbers including spin. For large Euclidean time separations t and $t_f - t$, the ground state propagation dominates the correlator:

$$\begin{aligned} G_{\sigma\tau}(\Gamma^\nu, \vec{p}, t) &= \frac{M_\Delta}{E_{\Delta(p)}} |Z|^2 e^{-E_{\Delta(p)}t} \operatorname{tr}[\Gamma^\nu \Lambda^E_{\sigma\tau}(p)] + \text{excited states} \\ G^{\mathrm{A}}_{\sigma\mu\tau}(\Gamma^\nu, \vec{q}, t; t_f) &= \frac{M_\Delta}{E_{\Delta(p)}} |Z|^2 e^{-M_\Delta(t_f - t)} e^{-E_{\Delta(p)}t} \operatorname{tr}[\Gamma^\nu \Lambda^E_{\sigma\sigma'}(0) \mathcal{O}^{E,A}_{\sigma'\mu\tau'} \Lambda^E_{\tau\tau'}(p)] + \text{excited states} \\ G^{\mathrm{PS}}_{\sigma\tau}(\Gamma^\nu, \vec{q}, t; t_f) &= \frac{M_\Delta}{E_{\Delta(p)}} |Z|^2 e^{-M_\Delta(t_f - t)} e^{-E_{\Delta(p)}t} \operatorname{tr}[\Gamma^\nu \Lambda^E_{\sigma\sigma'}(0) \mathcal{O}^{E,\mathrm{PS}}_{\sigma'\tau'} \Lambda^E_{\tau'\tau}(p)] + \text{excited states.} \end{aligned} \tag{33}$$

The Wick-rotated axial and pseudoscalar operators take the form

$$\mathcal{O}^{E,A}_{\sigma\mu\tau} = \frac{1}{2}\bigg[\delta_{\sigma\tau}\bigg(g_1(Q^2)\gamma_\mu\gamma_5 - i\frac{g_3(Q^2)}{2M_\Delta}Q_\mu\gamma_5\bigg) - \frac{Q^E_\sigma Q^E_\tau}{(2M_\Delta)^2}\bigg(h_1(Q^2)\gamma_\mu\gamma_5 - i\frac{h_3(Q^2)}{2M_\Delta}Q_\mu\gamma_5\bigg)\bigg], \tag{34}$$

$$\mathcal{O}^{E,\mathrm{PS}}_{\sigma\tau} = \frac{1}{2}\bigg[\delta_{\sigma\tau}(\tilde{g}(Q^2)\gamma_5) - \frac{Q_\sigma Q_\tau}{(2M_\Delta)^2}(\tilde{h}(Q^2)\gamma_5)\bigg], \tag{35}$$

with the Euclidean four-momentum transfer $Q_\mu = (i(M_\Delta - E_{\Delta(p)}), -\vec{q})$. The Rarita-Schwinger spin-sum relation becomes

$$\Lambda^E_{\sigma\tau} = -\frac{-i\not{p} + M_\Delta}{2M_\Delta}\bigg(\delta_{\sigma\tau} - \frac{\gamma_\sigma\gamma_\tau}{3} + \frac{2p_\sigma p_\tau}{3M_\Delta^2} - i\frac{p_\sigma\gamma_\tau - p_\tau\gamma_\sigma}{3M_\Delta}\bigg), \tag{36}$$

where all the γ matrices are in Euclidean space: $\gamma_0 = \gamma_4$ and $\gamma^M_k = -i\gamma^E_k$.

Forming an appropriate ratio of the three-point to the two-point correlator serves to cancel out the unknown Z factors and leading time dependence. A particular product of two-point correlators, which minimizes the denominator noise level, is used, as it contains smaller time extents. The proposed ratios are

$$R^A_{\sigma\mu\tau}(\Gamma^\nu, \vec{Q}, t) = \frac{G^A_{\sigma\mu\tau}(\Gamma, \vec{Q}, t)}{G_{kk}(\Gamma^4, \vec{0}, t_f)}\sqrt{\frac{G_{kk}(\Gamma^4, \vec{p}_i, t_f - t)G_{kk}(\Gamma^4, \vec{0}, t)G_{kk}(\Gamma^4, \vec{0}, t_f)}{G_{kk}(\Gamma^4, \vec{0}, t_f - t)G_{kk}(\Gamma^4, \vec{p}_i, t)G_{kk}(\Gamma^4, \vec{p}_i, t_f)}} \tag{37}$$

and

$$R^{\mathrm{PS}}_{\sigma\tau}(\Gamma^\nu, \vec{Q}, t) = \frac{G^{\mathrm{PS}}_{\sigma\tau}(\Gamma, \vec{Q}, t)}{G_{kk}(\Gamma^4, \vec{0}, t_f)}\sqrt{\frac{G_{kk}(\Gamma^4, \vec{p}_i, t_f - t)G_{kk}(\Gamma^4, \vec{0}, t)G_{kk}(\Gamma^4, \vec{0}, t_f)}{G_{kk}(\Gamma^4, \vec{0}, t_f - t)G_{kk}(\Gamma^4, \vec{p}_i, t)G_{kk}(\Gamma^4, \vec{p}_i, t_f)}}, \tag{38}$$

for the axial and pseudoscalar vertices. Summation over $k = 1, 2, 3$ is implicit in the two-point correlators. At large Euclidean time separations $t_f - t$ and t, these ratios become time independent (plateau region),

$$R^X_{\sigma(\mu)\tau}(\Gamma^\nu, \vec{Q}, t) \to C\Pi^X_{\sigma(\mu)\tau} = C \operatorname{tr}[\Gamma^\nu \Lambda_{\sigma\sigma'}(0)\mathcal{O}^X_{\sigma(\mu)\tau}\Lambda_{\tau'\tau}(p)], \tag{39}$$

where X stands for the axial (A_μ) or pseudoscalar (P) current. It is easy to show that the two-point correlators are dominated by

$$G_{kk}(\Gamma^4, \vec{p}, t) = |Z|^2 e^{-E_{\Delta(p)}t}\frac{E_{\Delta(p)} + M_\Delta}{E_{\Delta(p)}}\bigg(1 + \frac{\vec{p}^2}{3M_\Delta^2}\bigg), \tag{40}$$

and therefore the constant C is determined as

$$C \equiv \sqrt{\frac{3}{2}}\left[\frac{2E_{\Delta(p_i)}}{M_\Delta} + \frac{2E^2_{\Delta(p_i)}}{M^2_\Delta} + \frac{E^3_{\Delta(p_i)}}{M^3_\Delta} + \frac{E^4_{\Delta(p_i)}}{M^4_\Delta}\right]^{-\frac{1}{2}}. \quad (41)$$

There are at most 256 available combinations of the Dirac and Lorentz indices in Eq. (39), each one expressed as a linear combination of the axial (pseudoscalar) form factors times the kinematical tensor coefficients. Since we are interested in the momentum dependence of the matrix elements, evaluation of the three-point correlators is required for a large set of transition momenta $\vec{q}$ for both A_μ and P operators. In order to perform this economically, we use the sequential inversion through the sink technique [24] by fixing the sink time slice t_f and performing a backward sequential inversion through the sink. The sequential vector is coupled with a forward quark propagator and the Fourier transformed insertion operator at all intermediate time slices $0 \leq t \leq t_f$ at a small computational cost, obtaining thus the full momentum dependence of the amplitude. A drawback in this approach is the fact that the quantum numbers of the source and sink interpolators—which correspond to the Lorentz indices σ, τ, and Γ^ν—are now fixed per sequential inversion. Within the space of 64 available three-point correlators corresponding to choices of σ, τ, and ν, we perform an optimization by forming appropriate linear combinations such as the degree of rotational symmetry of the summed correlator is maximal, and consequently all transition momentum vectors $\vec{q}$ that correspond to a fixed virtuality q^2 will contribute to the form factor measurement in a rotationally symmetric fashion. This optimization technique has proven extremely useful in obtaining high-accuracy results in the nucleon elastic, nucleon-to-Δ electromagnetic [23], axial, and pseudoscalar transitions [22] as well as the Δ electromagnetic form factors [24]. We evaluate the Dirac traces in Eq. (39) using symbolic software such as `form` [29] and Mathematica.

We construct the following two optimal linear combinations, which we refer to as type I and type II:

$$\text{Type-I: } \Pi^{IA}_\mu(Q) \equiv \sum_{i=1}^{3}\sum_{\sigma,\tau=1}^{3}\delta_{\sigma\tau}\mathrm{tr}[\Gamma^i\Lambda_{\sigma\sigma'}(0)\mathcal{O}^{E,A}_{\sigma'\mu\tau'}\Lambda_{\tau'\tau}(p)] \quad (42)$$

$$\text{Type-II: } \Pi^{IIA}_\mu(Q) \equiv \sum_{\sigma,\tau=1}^{3}T_{\sigma\tau}\mathrm{tr}[\Gamma^4\Lambda_{\sigma\sigma'}(0)\mathcal{O}^{E,A}_{\sigma'\mu\tau'}\Lambda_{\tau'\tau}(p)], \quad (43)$$

with the matrix T,

$$T_{\sigma\tau} = \begin{bmatrix} 0 & 1 & -1 \\ -1 & 0 & 1 \\ 1 & -1 & 0 \end{bmatrix}. \quad (44)$$

Detailed expressions for the decomposition of the above combinations to the four axial form factors are provided in Appendix B. The above types are in addition used for the extraction of the two pseudoscalar couplings (Appendix B). A large number ($O(10^3)$) of correlators of axial (A_μ, $\mu = 1, 2, 3, 4$) and pseudoscalar (P) insertion momenta $\vec{q}$ are combined for momentum transfers ranging up to $\sim 3\ \mathrm{GeV}^2$ per ensemble. We stress that only two sequential inversions through sink—one for each type above—are required in order to disentangle completely all six form factors from the relevant three-point functions.

Correlators corresponding to a fixed momentum transfer q^2 are analyzed simultaneously in an overconstrained system analysis for the extraction of the form factors. Typically $O(20$–$50)$ plateau averages for the optimal ratios given in Eq. (39) will contribute to the determination of the form factor for each Q^2 value. A global χ^2 minimization amounts technically to the singular value decomposition of an $N \times M$ overcomplete linear system, with M unknowns (four for the axial or two for the pseudoscalar) and N input data [the $O(20$–$50)$ plateau averages]. Further details on this kind of analysis can be found in Ref. [30]. Jackknife estimates are used for all levels of variance extraction on the observables.

B. Ensembles and parameters

In Table I we summarize the parameters and number of configurations for the ensembles used in this work. As can be seen, three sets are employed. These are the same as the ones we used previously for the study of the nucleon axial form factors as well as the nucleon-to-Δ axial transition form factors. Therefore, these ensembles provide a complete calculation of the nucleon/Δ sector, allowing a direct extraction of low-energy couplings from a combined fit.

The gauge configurations used in the analysis include a set of quenched configurations on a $32^3 \times 64$, at $\beta = 6.0$, corresponding to a lattice spacing $a = 0.092$ fm with pion masses 560, 490, and 411 MeV. The low statistical noise makes this ensemble appropriate for checking our lattice methodology and some of the phenomenological relations. We apply Gaussian smearing at the source and sink in order to minimize the excited state contamination on the baryon correlators. The parameters $\alpha = 4.0$ and $n = 50$ have been tuned to provide optimal overlap to a nucleon state [22]. The source-sink separation is set at $\Delta T = 12a = 1.1$ fm. In our previous studies involving the Δ, such a time separation was found sufficient for ground state dominance. We show in Fig. 1 the ratios $R^{IA}_\mu(\vec{Q}, t) = \sum_{i=1}^3\sum_{\sigma=1}^3 R^A_{\sigma\mu\sigma}(\Gamma^i, \vec{Q}, t)$ and $R^{IIA}_\mu(\vec{Q}, t) = \sum_{\sigma,\tau=1}^3 T_{\sigma\tau}R^A_{\sigma\mu\tau}(\Gamma^4, \vec{Q}, t)$ corresponding to the two linear combinations that we considered in this work for the axial-vector current as given in Eqs. (42) and (43). As can be seen, one can identify a plateau range for various momenta $\vec{q} = -\vec{p}$ from where the matrix element can be extracted.

TABLE I. Ensembles and parameters used in this work. We give in the first column the lattice size; in the second the statistics; in the third, fourth, and fifth the pion, nucleon, and Δ mass in GeV, respectively. We did not do a full form-factor analysis on the $20^3 \times 64$ mixed-action ensemble. Rather we merely determined the axial matrix element at $q^2 = 0$ (a much cheaper computation) for our axial charge chiral fits.

V	Statistics	m_π (GeV)	m_N (GeV)	m_Δ (GeV)	κ
Quenched Wilson fermions					
$\beta = 6.0$, $a^{-1} = 2.14(6)$ GeV					
$32^3 \times 64$	200	0.563(4)	1.267(11)	1.470(15)	0.1554
$32^3 \times 64$	200	0.490(4)	1.190(13)	1.425(16)	0.1558
$32^3 \times 64$	200	0.411(4)	1.109(13)	1.382(19)	0.1562
Mixed action, $a^{-1} = 1.58(3)$ GeV					
Asqtad ($am_{\mathrm{u,d/s}} = 0.02/0.05$), DWF ($am_{\mathrm{u,d}} = 0.0313$)					
$20^3 \times 64$	264	0.498(3)	1.261(17)	1.589(35)	
Asqtad ($am_{\mathrm{u,d/s}} = 0.01/0.05$), DWF ($am_{\mathrm{u,d}} = 0.0138$)					
$28^3 \times 64$	550	0.353(2)	1.191(19)	1.533(27)	
DWFs					
$m_{\mathrm{u,d}}/m_s = 0.004/0.03$, $a^{-1} = 2.34(3)$ GeV					
$32^3 \times 64$	1428	0.297(5)	1.27(9)	1.455(17)	

The second set consists of two ensembles that use two degenerate light and one strange ($N_f = 2 + 1$) Asqtad-improved dynamical staggered fermions generated by the MILC Collaboration [31]. The strange quark mass is fixed to its physical value, the lattice spacing is set to 0.124 fm, and the lowest pion mass is 353 MeV. Our calculation employs domain wall valence quarks with light quark mass tuned so the pion mass matches the lowest pion mass obtained using staggered fermions. The extent of the fifth dimension of the domain wall action is set to $L_5 = 16a$, which was demonstrated to provide minimal violations to the chiral symmetry properties of the domain wall fermion (DWF) operator. The source-sink separation is set to $\Delta T = 8a = 1.0$ fm, and Gaussian smearing is applied at the source and sink with APE smearing [32] on gauge links that enter the smearing function applied on the interpolating fields. The parameters are given in Ref. [22]. Finally, the third set is an $N_f = 2 + 1$ ensemble of DWF generated by the RBC-UKQCD collaborations [33] with a lattice spacing $a = 0.084$ fm and the physical volume of $(2.7\ \mathrm{fm})^3$ and a pion mass of 0.297 MeV. The extent of the fifth dimension is also $L_5 = 16a$ here. It turns out that the residual quark mass introduced via the chiral symmetry breaking effects is $am_{\mathrm{res}} = 0.000665(3)$, or 17% of the bare quark mass. The smearing parameters for the interpolating fields are given in Ref. [23]. The sink-source time separation is set at $\Delta T = 12a = 1.01$ fm. In order to increase the statistics at this lowest pion mass, we use the coherent sink technique, employed in our study of the nucleon-to-Δ transition using the same ensemble [23]. The four quark sources are placed at time slice $t_i = (i-1)16$, $i = 1, \ldots, 4$ for each configuration. Four forward propagators must be computed—each with a source at one of the time slices. The Δ sinks are constructed at all

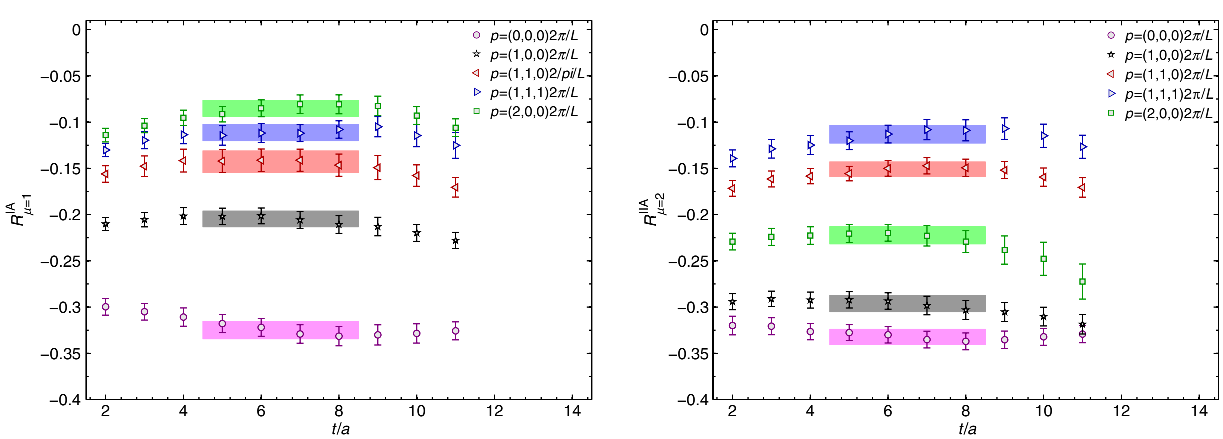

FIG. 1 (color online). The unrenormalized ratios that yield the plateaus given in Eqs. (42) and (43) are shown for type I and current direction $\mu = 1$ (left) and type II and current direction $\mu = 2$ (right) for various values of the momentum.

four equally spaced time slices $t_f(i) = t_i + 12$, and one sequential inversion is performed in order to construct the three-point correlator. Gauge invariance ensures that combining the sequential vector with each one of the forward quark propagators generated at t_i projects the appropriate Δ matrix element between t_i and $t_i + 12$ as the other cross terms will average to zero. It has been shown in Ref. [23] that while statistics is thus multiplied by four, the noise level is not raised above what is expected from the four completely independent correlators that participate in the coherent sink. This means that we can reduce the error by a factor of two at the cost of one sequential inversion. Therefore, the 1428 statistics given in the table correspond to 357 coherent sequential inversions per each type of combination [see Eqs. (42) and (43)].

IV. RESULTS

A. Axial-vector and pseudoscalar form factors

In this section we present results on the Δ axial-vector and pseudoscalar form factors from the ensembles used in this work. The axial current is renormalized multiplicatively in all ensembles. Values for the renormalization constant Z_A are provided in Table II.

In Figs. 2–5, we show the results for the four axial form factors, g_1, g_3, h_1, and h_3, respectively. All the results on these form factors are provided in Appendix C (Tables XI, XII, XIII, XIV, and XV). The form factor g_1 is the dominant axial-vector form factor and the only one that can be extracted directly from the matrix element at $Q^2 = 0$, determining the axial charge of the Δ. Based on the PCAC and pion-pole dominance, we expect g_1 to be a smooth function of Q^2, whereas h_1 and g_3 to have a pion-pole and h_3 a double pion-pole behavior. Given that g_1 and h_1 are multiplied by Q^2, whereas h_3 is multiplied by Q^4, it is increasingly more difficult to resolve these form factors via the simultaneous overconstrained analysis of the measured matrix element of the axial-vector current,

TABLE II. The first column gives the hopping parameter κ for Wilson fermions or the lattice mass of the domain wall fermion, the second the renormalized quark mass, the third the unrenormalized pion decay constant f_π/Z_A in lattice units, and the fourth the axial current renormalization constant Z_A.

κ or am_l	am_q	af_π/Z_A	Z_A
	Quenched Wilson fermions		
0.1554	0.0403(4)	0.0611(14)	0.808(7)
0.1558	0.0307(4)	0.0587(16)	0.808(7)
0.1562	0.0213(4)	0.0563(17)	0.808(7)
	Hybrid or mixed action		
0.02	0.0324(4)	0.0648(8)	1.0994(4)
0.01	0.0159(2)	0.0636(6)	1.0847(6)
	$N_F = 2 + 1$ DWF		
0.004	0.004665(3)	0.06575(12)	0.74521(2)

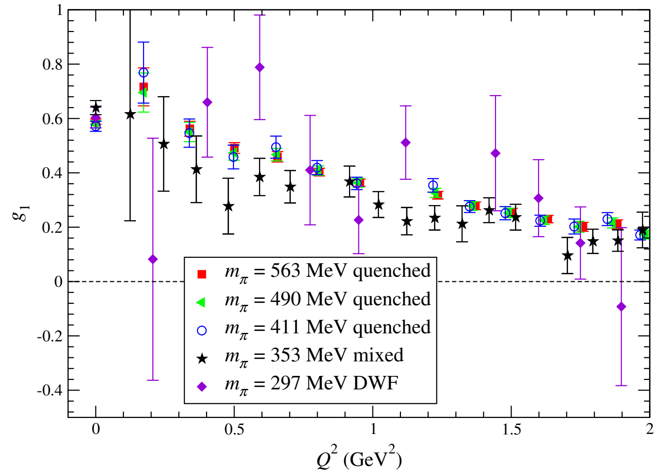

FIG. 2 (color online). Lattice QCD results for the g_1 axial form factor.

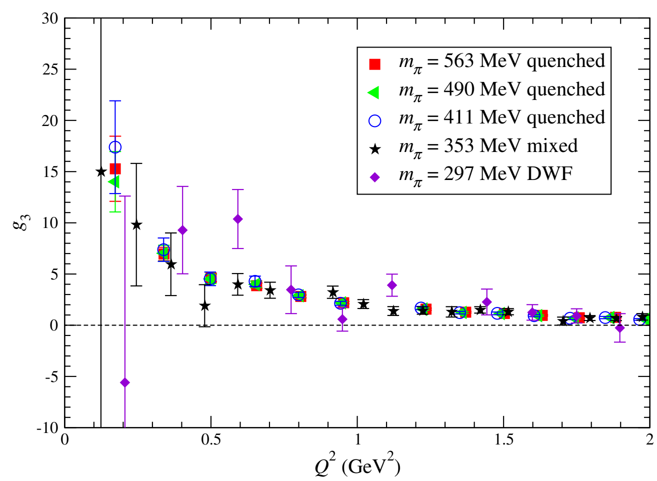

FIG. 3 (color online). Lattice QCD results for the g_3 axial form factor.

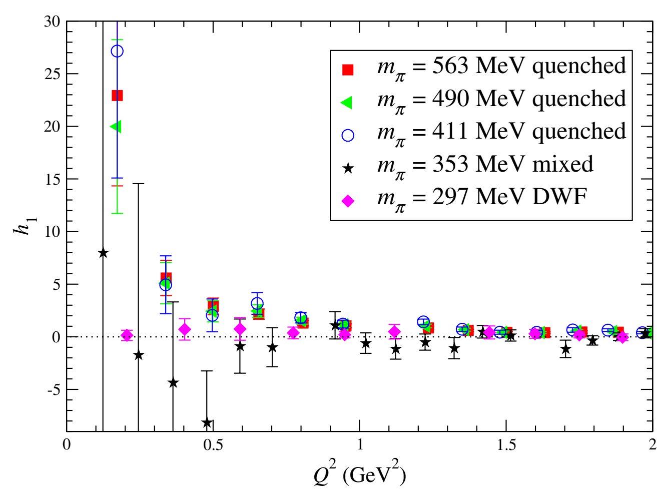

FIG. 4 (color online). Lattice QCD results for the h_1 axial form factor.

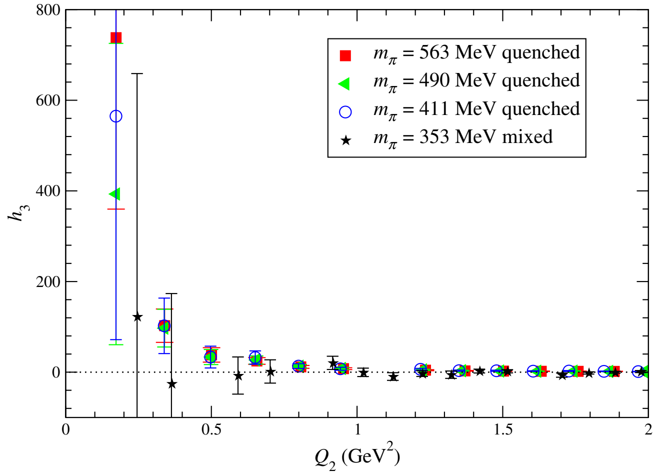

FIG. 5 (color online). Lattice QCD results for the h_3 axial form factor.

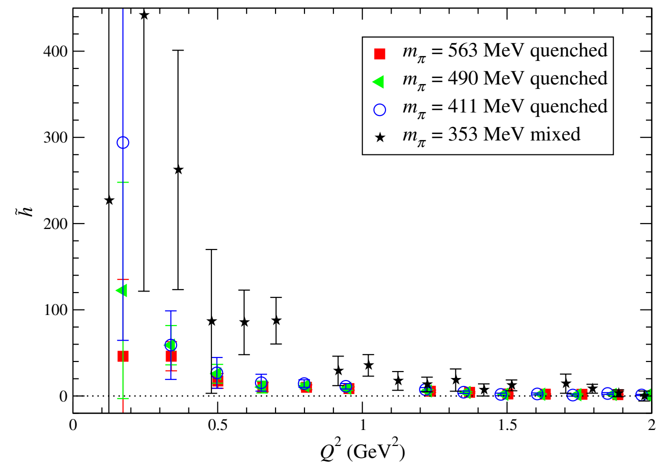

FIG. 7 (color online). Lattice QCD results for the $\tilde{h}$ pseudoscalar form factor.

especially at small Q^2—a fact that is clearly reflected on the statistical error of the form factors shown in the figures. The results from the quenched ensemble, although based on the analysis of 200 configurations, have the lowest statistical noise, and this is the primary reason for using them in this first calculation of the form factors. The statistical noise is more severe for the DWF ensemble at $m_\pi = 297$ MeV, for which results on h_3 are too noisy to be useful and are omitted from plots. We do, however, include these numbers in the tables in Appendix C for completeness.

Figures 6 and 7 show the pseudoscalar form factors $\tilde{g}$ and $\tilde{h}$, respectively, as defined in Eq. (10), where the pion pole is explicitly written. The numerical values of these form factors are provided in Appendix C. As confirmed by the numerical results, $\tilde{g}$ is the dominant pseudoscalar form factor showing a pion-pole dependence, whereas the subdominant form factor $\tilde{h}$ shows a stronger Q^2 dependence consistent with a double pion pole. In Sec. II we already defined the physically relevant pion-Δ coupling $G_{\pi\Delta\Delta}(m_\pi^2)$, factoring out the pion pole and fixing coefficients via the PCAC through Eq. (14). $G_{\pi\Delta\Delta}(q^2)$ has a finite value at the origin, as can be seen in Fig. 8, where numerical results are depicted. This value in fact defines the traditional strong coupling $g_{\pi\Delta\Delta}$ of the pion to the Δ state via

$$g_{\pi\Delta\Delta} = G_{\pi\Delta\Delta}(m_\pi^2). \tag{45}$$

The secondary momentum-dependent coupling, $H_{\pi\Delta\Delta}(Q^2)$, is plotted in Fig. 9. The numerical results are consisted with a pion-pole divergence at small Q^2, as expected from the analysis given in the previous section. The statistical error on this coupling is larger in particular at small Q^2 since, in the combined analysis, the pseudoscalar matrix element is multiplied by a factor of Q^2.

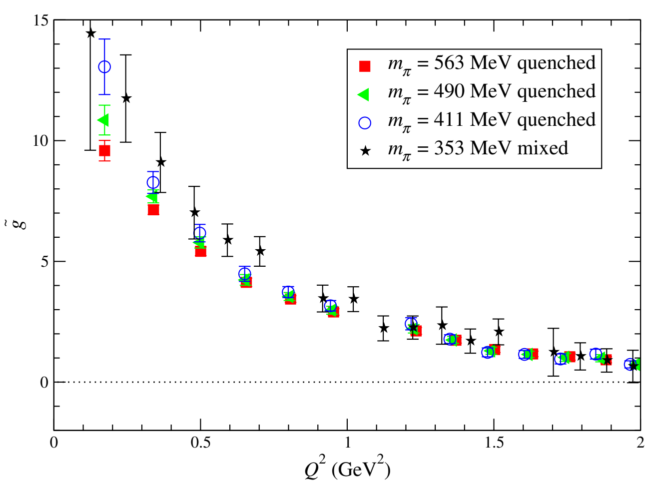

FIG. 6 (color online). Lattice QCD results for the $\tilde{g}$ pseudoscalar form factor.

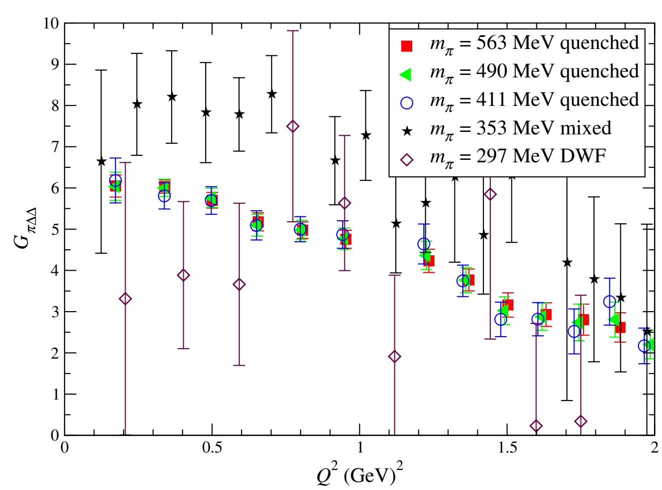

FIG. 8 (color online). Lattice QCD results for the primary $\pi\Delta\Delta$ coupling, $G_{\pi\Delta\Delta}$.

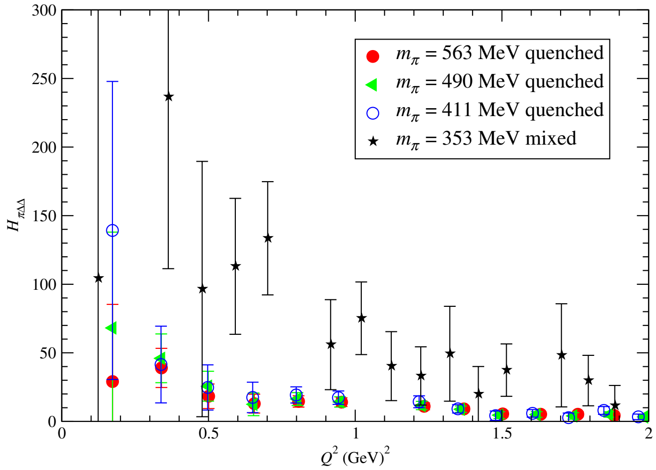

FIG. 9 (color online). Lattice QCD results for the secondary $\pi\Delta\Delta$ coupling, $H_{\pi\Delta\Delta}$.

Notice that the extraction of $G_{\pi\Delta\Delta}$ and $H_{\pi\Delta\Delta}$ from Eqs. (14) and (15) requires knowledge of the light quark mass m_q and the pion decay constant, f_π, on each of the ensembles. The calculation of f_π requires the two-point functions of the axial-vector current A_4^3 with local-smeared (LS) and smeared-smeared (SS) quark sources,

$$C_{\rm LS}^A(t) = \sum_{\mathbf{x}} \langle\Omega|T(A_4^3(\mathbf{x},t)\tilde{A}_4^3(\mathbf{0},0))|\Omega\rangle \tag{46}$$

(and similarly for $C_{\rm SS}^A$), where $A_4^3(\mathbf{x},t)$ denotes the local operator and $\tilde{A}_4^3(\mathbf{x},t)$ the smeared operator. The pion decay constant f_π is obtained from the pion-to-vacuum matrix element,

$$\langle 0|A_\mu^a(0)|\pi^b(p)\rangle = if_\pi p_\mu \delta^{ab}, \tag{47}$$

extracted from the ratio of the two-point functions $C_{\rm LS}^A$ and $C_{\rm SS}^A$ and

$$f_\pi^{\rm eff}(t) = Z_A\sqrt{\frac{2}{m_\pi}}\frac{C_{\rm LS}^A(t)}{\sqrt{C_{\rm SS}^A(t)}}e^{m_\pi t/2} \tag{48}$$

in the large Euclidean time limit.

The renormalized quark mass m_q is determined from AWI, via two-point functions of the pseudoscalar density with either local (P^3) or smeared ($\tilde{P}^3$) quark fields,

$$C_{\rm LS}^P(t) = \sum_{\mathbf{x}} \langle\Omega|T(P^3(\mathbf{x},t)\tilde{P}^3(\mathbf{0},0))|\Omega\rangle \tag{49}$$

(and similarly for $C_{\rm SS}^P$). The effective quark mass is defined by

$$m_{\rm eff}^{\rm AWI}(t) = \frac{m_\pi}{2}\frac{Z_A}{Z_P}\frac{C_{\rm LS}^A(t)}{C_{\rm LS}^P(t)}\sqrt{\frac{C_{\rm SS}^P(t)}{C_{\rm SS}^A(t)}}, \tag{50}$$

and its plateau value yields m_q. Note that Z_P will be needed only if ones wants m_q alone. Since Z_P enters also Eq. (13), it cancels—as does Z_A since it comes with f_π—and therefore $G_{\pi\Delta\Delta}$ and $H_{\pi\Delta\Delta}$ are extracted directly from ratios of lattice three- and two-point functions without prior knowledge of either Z_A or Z_P. We also note that the quark mass computed through Eq. (50) includes the effects of residual chiral symmetry breaking from the finite extent L_5 of the fifth dimension. These effects are of the order of 17% for the DWF ensemble and 15% for the hybrid ensemble (also referred to as the mixed scheme). Chiral symmetry breaking affects the PCAC relations and therefore the value of both strong couplings $G_{\pi\Delta\Delta}$ and $H_{\pi\Delta\Delta}$ through Eq. (13).

B. Testing pion-pole dominance in the axial and pseudoscalar matrix element

In this section we examine in detail the pion-pole dependence expected for the Δ form factors by performing fits to the results obtained. First, we test the validity of the Goldberger-Treiman relations of Eqs. (23) and (24) by evaluating the ratios

$$\frac{f_\pi G_{\pi\Delta\Delta}(q^2)}{M_\Delta g_1(q^2)} \tag{51}$$

and

$$\frac{f_\pi H_{\pi\Delta\Delta}(q^2)}{M_\Delta h_1(q^2)}. \tag{52}$$

These relations are expected to hold at low Q^2. We show the results in Figs. 10 and 11. The first ratio, given in Eq. (51), carries moderate statistical error. It is consistent with unity for $Q^2 \gtrsim 0.8$ GeV^2 for the quenched ensembles while it is underestimated at smaller Q^2 values. This discrepancy at smaller Q^2 can be attributed to chiral effects on $G_{\pi\Delta\Delta}$, which is expected to be more seriously affected by pion cloud effects than g_1. The results using the hybrid dynamical ensemble, on the other hand, are consistently higher than unity for $Q^2 > 0.5$ GeV^2. The large statistical

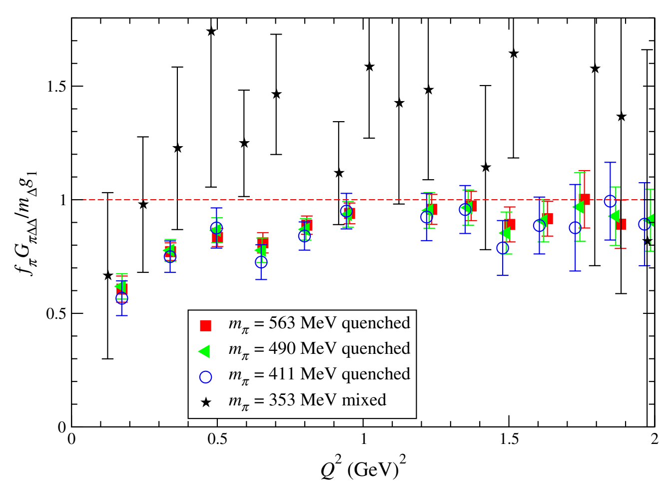

FIG. 10 (color online). Ratio test of the Goldberger-Treiman relation for $G_{\pi\Delta\Delta}$.

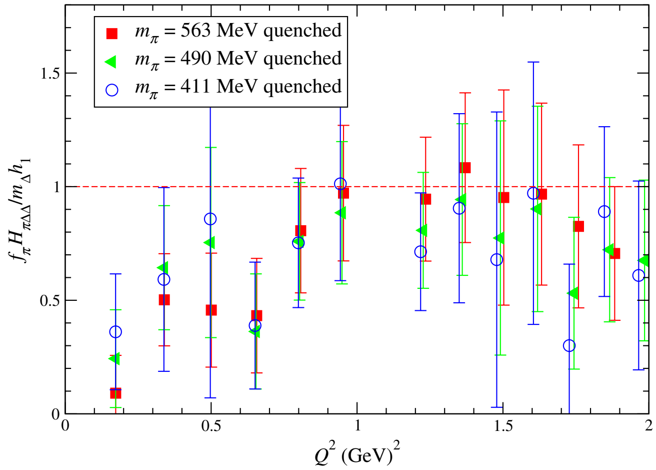

FIG. 11 (color online). Ratio test of the Goldberger-Treiman relation for $H_{\pi\Delta\Delta}$.

errors carried by these data make it difficult to draw definite conclusions. The behavior of this ratio is very similar to the behavior shown by the corresponding ratio for the nucleon GT relation as well as the nucleon-to-Δ axial transition [22].

The second GT-type relation, given in Eq. (52), is statistically consistent with unity for the quenched results and $Q^2 > 0.8$ GeV^2. The results from the dynamical ensembles are plagued by too large statistical noise to be able to meaningfully display them on the plot. We therefore have omitted these data from Fig. 11. A very similar and consistent behavior with the first ratio is observed for the quenched data. We remind the reader that it is the first Goldberger-Treiman relation that is more significant for phenomenology, as it is this relation that connects the axial charge (from g_1 at $Q^2 = 0$) to the $G_{\pi\Delta\Delta}$ coupling.

To further probe the pion pole assumptions entering into our derivation of the GT relations, we perform a set of fits to our form factor data. We have no *a priori* theoretical expectation for the functional form of $g_1(q^2)$, although typically a dipole form seems to accommodate well the nucleon axial form factor G_A as well as the leading axial N-Δ transition form factor C_5^A. We note, however, that there seems to be a small dip in the g_1 at $q^2 = 0$ for the quenched ensembles. To accommodate this we fit the data to

$$g_1(Q^2) = \frac{a + bQ^2}{(Q^2 + m_1^2)^3}. \tag{53}$$

The resulting fits are shown in Fig. 12. The values for the fitted parameters are given in Table III. We note that the mass parameter m_1 determining the slope as $Q^2 \to 0$ is around 1 GeV, a scale typical for axial dipole masses controlling the dependence of nucleon G_A and the dominant axial N-Δ C_5^A form factor.

We consider the form

$$\left[\frac{a + bQ^2}{(Q^2 + m_1^2)^3}\right]\frac{c}{(Q^2 + m_2^2)} \tag{54}$$

for g_3 based on the pion-pole dominance prediction given in Eq. (25). The parameters a, b, and m_1 are fixed to the

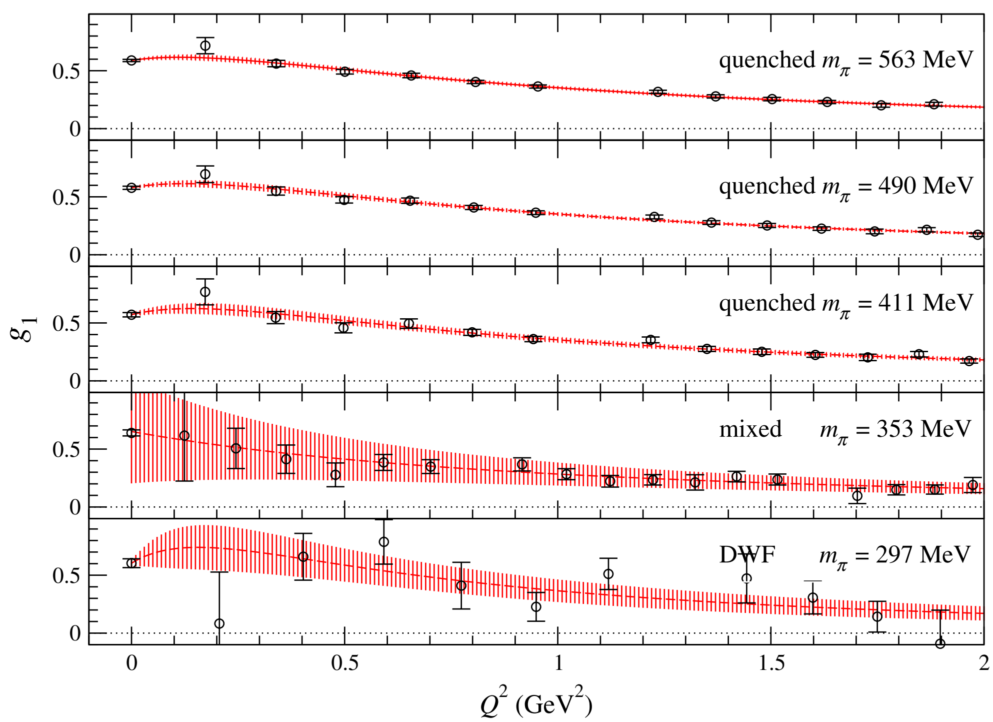

FIG. 12 (color online). Fits to the data for the g_1 form factor using the form given in Eq. (53).

TABLE III. Fit parameters for $g_1(Q^2)$ using Eq. (53).

m_π (GeV)	a	b	m_1 (GeV)	χ^2/dof
Quenched Wilson fermions				
0.563	0.53(18)	2.15(31)	0.98(5)	0.82
0.490	0.47(18)	2.08(33)	0.99(6)	1.07
0.411	0.40(19)	1.98(38)	0.94(8)	1.48
Mixed action				
0.353	3.0(22.0)	2.4(1.9)	1.3(1.2)	0.44
Domain wall fermions				
0.297	0.19(24)	1.5(9)	0.82(18)	1.1

values arising from the fit of the g_1 data using the Ansatz given in Eq. (53). The fits are shown in Fig. 13. The fitted parameters are given in Table IV. Note that the value of m_2 is considerably smaller compared to m_1, as in fact is expected since this is detected from the presence of the pion pole. This is especially verified by the quenched data where m_2 is close to the actual pion mass m_π of the ensemble.

Pion-pole dominance fixes completely the ratio g_3/g_1

$$\frac{g_3}{g_1} = \frac{4M_\Delta^2}{m_\pi^2 - q^2}. \tag{55}$$

We form the ratio g_3/g_1 from our data and fit separately to a monopole form:

$$\frac{c}{(Q^2 + m_2^2)}. \tag{56}$$

TABLE IV. Fit parameters for $g_3(Q^2)$ using Eq. (54). Parameters a, b, and m_1 are fixed with the results of the g_1 fits in Table III.

m_π (GeV)	c	m_2 (GeV)	χ^2/dof
Quenched Wilson fermions			
0.563	7.77(88)	0.54(11)	0.61
0.490	7.45(89)	0.50(11)	0.55
0.411	7.1(1.0)	0.44(15)	0.65
Mixed action			
0.353	10.7(4.6)	0.67(43)	0.49
Domain wall fermions			
0.297	10.0(5.3)	0.56(37)	1.26

This fit is displayed in Fig. 14. Using a ratio eliminates any need to know the theoretical form for $g_1(q^2)$ alone. The fitted parameters c and m_2 are given in Table V. The verification of the predicted form given in Eq. (55) is very good, with the pole mass m_2 consistent with the pion mass and the constant c reasonably close to $4M_\Delta^2$.

The form factor h_1 is similar to g_3 having a pion-pole dependence. We display the ratio h_1/g_3 in Fig. 15 for the quenched QCD ensembles. This ratio is notably constant over the whole Q^2 range above 0.4 GeV^2, with the constant ~0.5. Based on this observation, we use the Ansatz given in Eq. (54) also for h_1. The fit is shown in Fig. 16, and the fitted parameters are given in Table VI. Again, m_2 is considerably smaller compared to m_1, in accordance with the presence of a light (pion) mode.

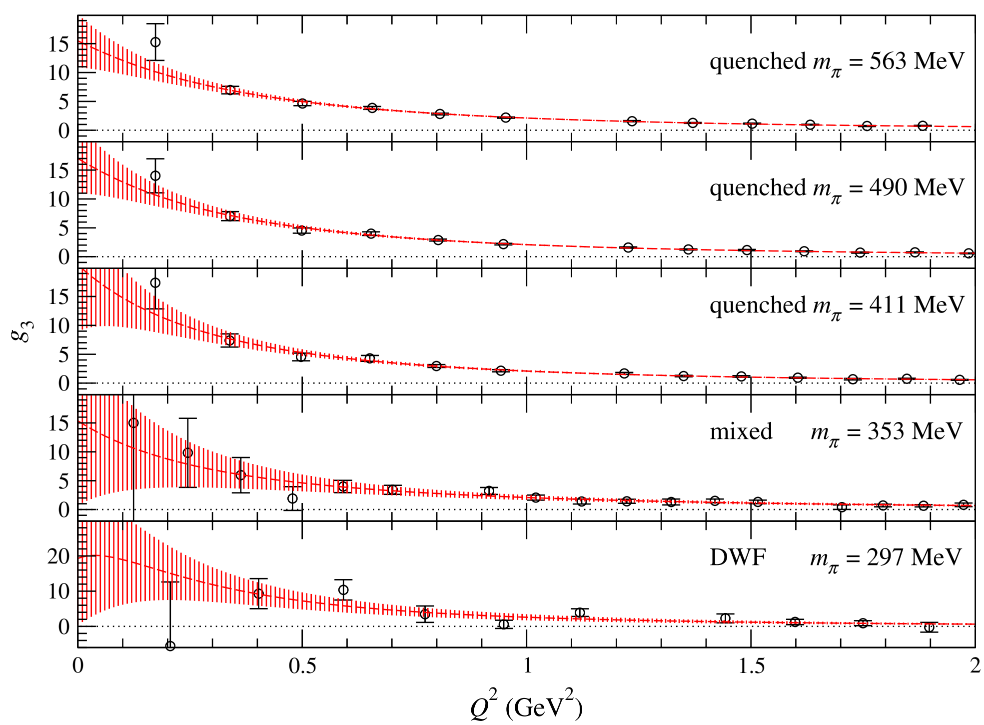

FIG. 13 (color online). Fits to the data for the g_3 form factor using the form given in Eq. (54).

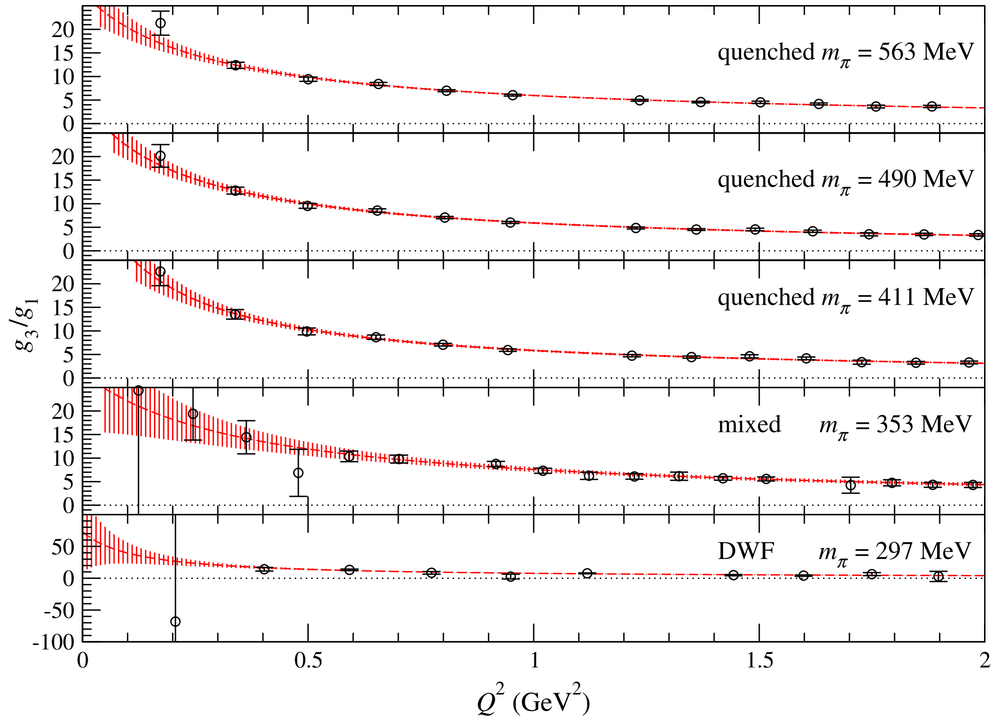

FIG. 14 (color online). Monopole fits as given by Eq. (56) to the ratio g_3/g_1.

From Eq. (26) the ratio h_3/h_1 is completely fixed:

$$\frac{h_3}{h_1} = \frac{4M_\Delta^2}{m_\pi^2 - q^2}. \tag{57}$$

We plot this ratio in Fig. 17. Fitting the data to the monopole form of Eq. (56), we get parameters m_2 and c within the range of the expected value (Eq. (57))—see Table VII indicating that the subdominant form factor diverges with a double pion-pole dependence.

In Fig. 18 we present the fit of h_3 to the Ansatz

$$\left[\frac{a + bQ^2}{(Q^2 + m_1^2)^3}\right]\frac{d}{(Q^2 + m_2^2)^2}, \tag{58}$$

TABLE V. Fit parameters for $g_3(Q^2)/g_1(Q^2)$ using the monopole form of Eq. (56).

m_π (GeV)	m_2 (GeV)	c	$4M_\Delta^2$ (GeV^2)	χ^2/dof
Quenched Wilson fermions				
0.563	0.523(64)	7.60(52)	8.64(18)	0.67
0.490	0.477(63)	7.25(49)	8.12(18)	0.54
0.411	0.396(75)	6.76(48)	7.64(21)	0.60
Mixed action				
0.353	0.61(18)	10.4(1.6)	9.40(33)	0.34
Domain wall fermions				
0.297	0.34(17)	8.6(1.3)	5.82(20)	0.66

with a, b, and m_1 fixed to the values extracted from the fit of g_1. The fitted parameters d and m_2 are given in Table VIII, in accordance to the h_3/h_1 fit (Table VII).

In the pseudoscalar sector, one expects a monopole dependence also for the ratio $\tilde{h}/\tilde{g}$. Fitting the data to the monopole form of Eq. (56), we get the parameters provided in Table IX. Indeed, we see an agreement between the pole mass m_2 and the pion mass within the statistical uncertainty.

The overall conclusion from the fits in this section is that all form factors satisfy qualitatively the pion-pole dependence predicted by the PCAC. This is most clearly exemplified in the case of quenched QCD where the level of statistical noise allows such a detailed analysis. In all cases the data fit these forms to good confidence levels, i.e., $\chi^2/\text{dof} \lesssim 1$. Enhanced statistical noise for the dynamical ensembles limits the verification to the dominant form factors only, as the subdominant ones are beyond reach, but this still is a useful result as it shows the consistency between quenched and dynamical results. This corroborates other baryon studies that show small effects due to a dynamical quark for pion masses larger than about 300 MeV.

V. PHENOMENOLOGICAL COUPLINGS OF THE Δ AND COMBINED CHIRAL FIT

Crucial parameters in heavy baryon chiral effective theories (HBχPT) with explicit Δ degrees of freedom are

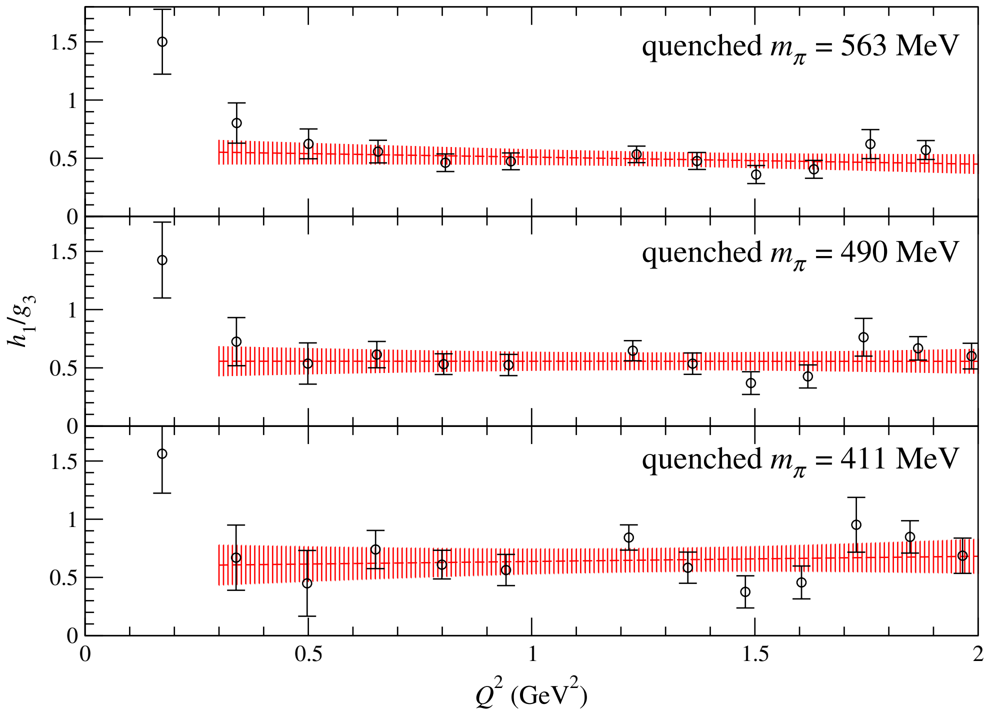

FIG. 15 (color online). The ratio h_1/g_3 as a function of Q^2, with unity marked with a red line.

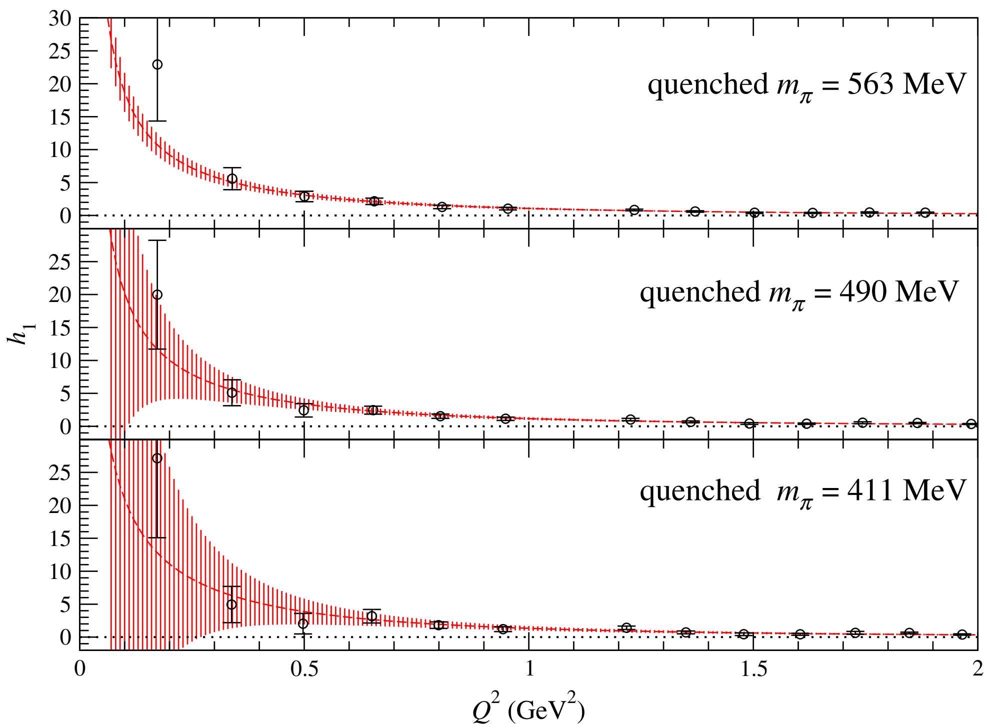

FIG. 16 (color online). Fits to the data for the h_1 form factor using the form given in Eq. (54).

the axial couplings of the nucleon, g_A, the axial N-Δ transition coupling, c_A, and the axial charge of the Δ, $g_{\Delta\Delta}$. Assuming the PCAC these can be related via GT relations to the effective πNN, $\pi N\Delta$, and $\pi\Delta\Delta$ strong couplings:

$$g_A = \frac{f_\pi}{M_N} g_{\pi NN}, \quad c_A = \frac{f_\pi}{M_N} g_{\pi N\Delta}, \quad g_{\Delta\Delta} = \frac{f_\pi}{M_\Delta} g_{\pi\Delta\Delta}. \tag{59}$$

We note that alternative notation and normalization factors exist in the literature in the definition of the

TABLE VI. Fit parameters for $h_1(Q^2)$ using Eq. (54). Parameters a, b, and m_1 are fixed with the results of the g_1 fits in Table III.

m_π (GeV)	c	m_2 (GeV)	χ^2/dof
Quenched Wilson fermions			
0.563	3.04(48)	$2\times10^{-8}(8\times10^{-7})$	1.32
0.490	3.32(84)	0.03(81)	1.37
0.411	3.8(1.8)	0.1(1.4)	1.52

TABLE VII. Fit parameters for $h_3(Q^2)/h_1(Q^2)$ using the monopole form of Eq. (56).

m_π (GeV)	m_2 (GeV)	c	$4M_\Delta^2$ (GeV^4)	χ^2/dof
Quenched Wilson fermions				
0.563	0.26(17)	7.6(1.1)	8.64(18)	0.21
0.490	0.31(19)	7.4(1.1)	8.12(18)	0.38
0.411	0.28(25)	6.7(1.1)	7.64(21)	0.58

effective strong couplings for $\pi N\Delta$ and $\pi\Delta\Delta$. In addition, note that in such schemes, Eqs. (59) are actually defining relations for the strong couplings. g_A is very well known experimentally, and a variety of lattice and theoretical calculations offer precise estimates. c_A is much less well determined, via the parity-violating N-to-Δ amplitude, which connects it to the dominant axial transition form factor $C_5^A(q^2)$. $g_{\Delta\Delta}$ remains undetermined from the experiment and is typically treated—as is also the case for c_A—as a fit parameter to be determined from fits to experimental or lattice data.

There have been several sum-rules calculations of the effective $\pi\Delta\Delta$ coupling [34–36]. In Ref. [37] symmetry arguments in a quartet scheme, where N_+^*, N_-^*, Δ_+, and Δ_- form a chiral multiplet, lead to the conclusion that $\pi\Delta_\pm\Delta_\pm$ couplings (with like-charged Δs) are forbidden at tree level. Quark-model arguments [20] suggest that $g_{\pi\Delta\Delta} = (4/5)g_{\pi NN}$. Recently an analysis of axial-vector couplings was studied in the framework of the combined $1/N_c$ and chiral expansions [38]. Results for the nucleon, Δ, and Δ-to-πN axial couplings are presented.

Lattice calculations for the nucleon axial charge g_A are available on a variety of ensembles and pion masses [27]. In addition, results on the axial N-Δ transition form factor C_5^A [23] have been obtained on most of the ensembles used also in this work. We are therefore in a position to perform a combined chiral fit using small scale expansion (SSE) within (HBχPT) [17,28,39] for g_A, $C_5^A(q^2)$ and the Δ axial charge $G_{\Delta\Delta}$ as functions of the pion mass m_π.

The one-loop SSE expression for C_5^A has been worked by Procura [39]. The expression for $C_5^A(q^2)$ as a function of m_π is

$$C_5^A = a_1 + a_2 m_\pi^2 + a_3 q^2 + \mathrm{loop}_5(m_\pi), \qquad (60)$$

where the loop integral contribution is

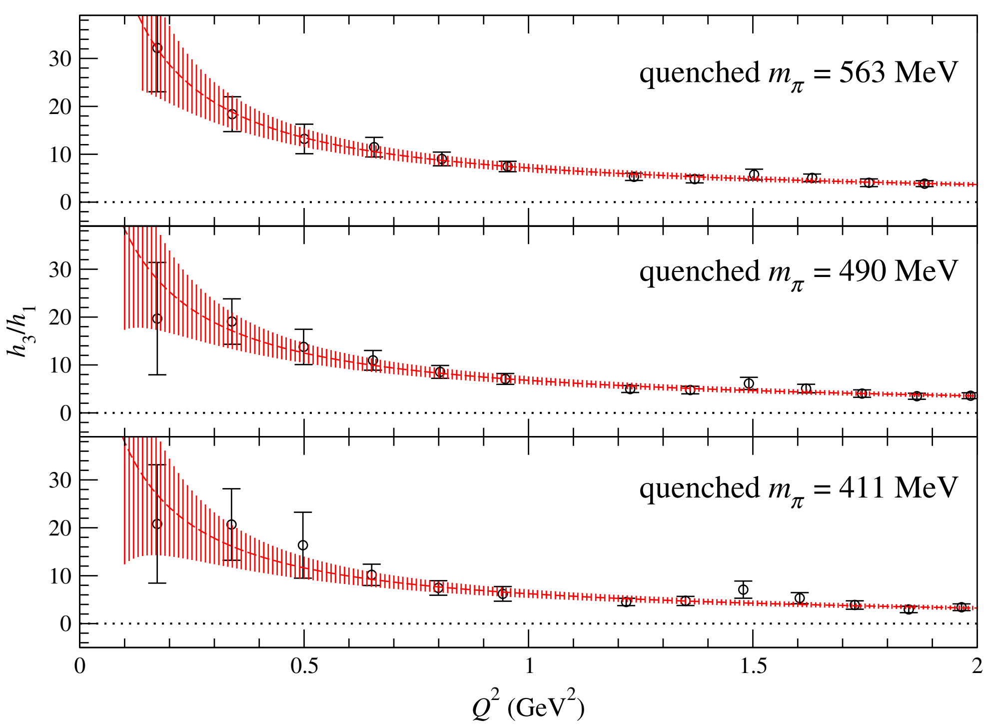

FIG. 17 (color online). Monopole fits to the ratio h_3/h_1 as described by Eq. (56).

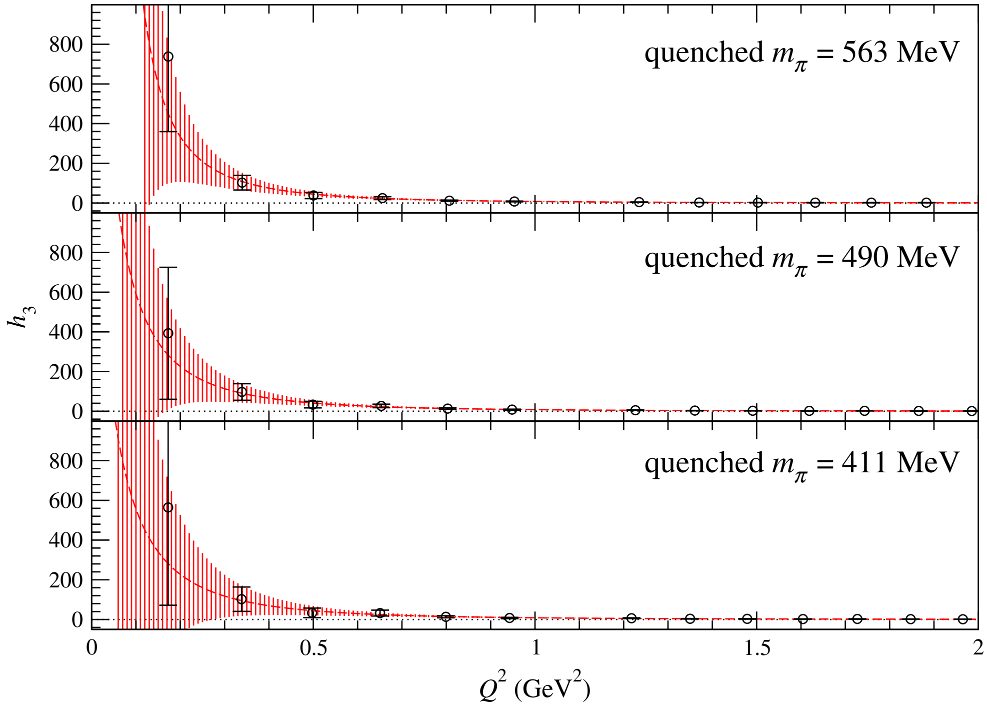

FIG. 18 (color online). Fits to the data for the h_3 form factor using the form given in Eq. (58).

$$\mathrm{loop}_5(m_\pi) = \frac{c_A}{15552\pi^2 f_\pi^2}\left\{\frac{1}{\Delta}\left[\frac{5}{4}g_{\Delta\Delta}^2(40\pi m_\pi^3 + 101\Delta m_\pi^2 + 24\Delta^3) + \frac{1170}{2}g_A g_{\Delta\Delta} m_\pi^2 \Delta - 12\Delta c_A^2(162 m_\pi^2 - 83\Delta^2) - 27 g_A^2(24\pi m_\pi^3 + 75\Delta m_\pi^2 - 40\Delta^3)\right] + \frac{72}{\Delta}\sqrt{m_\pi^2 - \Delta^2}(m_\pi^2 c_A^2 - 28\Delta^2 c_A^2 + 18 g_A^2(m_\pi^2 - \Delta^2))\arccos\left(-\frac{\Delta}{m_\pi}\right) - \frac{8}{\Delta}\sqrt{m_\pi^2 - \Delta^2}\left(9m_\pi^2 c_A^2 + 963\Delta^2 c_A^2 + \frac{50}{4}g_{\Delta\Delta}^2(m_\pi^2 - \Delta^2)\right)\arccos\left(\frac{\Delta}{m_\pi}\right) - \left[3m_\pi^2\left(900c_A^2 - \frac{425}{4}g_{\Delta\Delta}^2 - \frac{450}{2}g_{\Delta\Delta}g_A + 81 g_A^2 + 648\right) + 8\Delta^2\left(-711 c_A^2 + \frac{50}{4}g_{\Delta\Delta}^2 + 162 g_A^2\right)\right]\ln\left(\frac{m_\pi}{\lambda}\right)\right\}. \tag{61}$$

Here $\Delta = M_\Delta - M_N$, $f_\pi = 92.4$ MeV, a_1, a_2, a_3 are unknown parameters, and λ is a cutoff scale set to $\lambda = 1$ GeV.

We use the SSE expression for the nucleon axial charge presented in Ref. [40]:

$$g_A^{\mathrm{SSE}}(m_\pi^2) = g_A^0 - \frac{g_A^{0\,3} m_\pi^2}{16\pi^2 f_\pi^2} + 4\left[C^{\mathrm{SSE}}(\lambda) + \frac{c_A^2}{4\pi^2 f_\pi^2}\left(\frac{155}{1944}g_{\Delta\Delta} - \frac{17}{36}g_A^0\right) + \gamma^{\mathrm{SSE}}\ln\frac{m_\pi}{\lambda}\right]m_\pi^2 + \frac{4c_A^2 g_A^0}{27\pi f_\pi^2\Delta}m_\pi^3 + \frac{8}{27\pi^2 f_\pi^2}c_A^2 g_A^0 m_\pi^2\sqrt{1 - \frac{m_\pi^2}{\Delta^2}}\ln R + \frac{c_A^2\Delta^2}{81\pi^2 f_\pi^2}\left(\frac{25}{2}g_{\Delta\Delta} - 57 g_A^0\right)\left(\ln\frac{2\Delta}{m_\pi} - \sqrt{1 - \frac{m_\pi^2}{\Delta^2}}\ln R\right) + \mathcal{O}(\epsilon^4), \tag{62}$$

TABLE VIII. Fit parameters for $h_3(Q^2)$ using Eq. (58). Parameters a, b, and m_1 are fixed with the results of the g_1 fits in Table III. The dynamical fermion data sets contain too much noise for the fits to be useful.

m_π (GeV)	d	m_2 (GeV)	χ^2/dof
	Quenched Wilson fermions		
0.563	22(6)	0.03(58)	0.46
0.490	26(10)	0.25(28)	0.35
0.411	28(15)	0.28(43)	0.33

TABLE IX. Fit parameters for $\tilde{h}(Q^2)/\tilde{g}(Q^2)$ using the monopole form of Eq. (56).

m_π (GeV)	m_2 (GeV)	c	χ^2/dof
	Quenched Wilson fermions		
0.563	0.73(39)	4.2(1.6)	0.23
0.490	0.42(43)	3.3(1.2)	0.22
0.411	0.45(70)	3.9(2.0)	0.32

with

$$\gamma^{\rm SSE} = \frac{-1}{16\pi^2 f_\pi^2}\left[g_A^0\left(\frac{1}{2}+g_A^{0\,2}\right)+\frac{2}{9}c_A^2\left(g_A^0-\frac{25}{18}g_{\Delta\Delta}\right)\right], \qquad R = \frac{\Delta}{m_\pi}+\sqrt{\frac{\Delta^2}{m_\pi^2}-1}. \tag{63}$$

g_A^0 in the above expressions denotes the chiral limit value of the axial charge, i.e., corresponds to g_A in Eq. (61).

Finally, from Jiang and Tiburzi [28] we obtain the chiral expansion for the axial charge of the Δ:

$$G_{\Delta\Delta}(m_\pi^2) = g_{\Delta\Delta}Z_\Delta - \frac{1}{(4\pi f_\pi)^2}\left[g_{\Delta\Delta}\mathcal{L}(m_\pi,\mu)\left(1+\frac{121}{324}g_{\Delta\Delta}^2\right)+c_A^2\left(\frac{8}{9}g_{\Delta\Delta}\mathcal{K}(m_\pi,-\Delta,\mu)-g_A\mathcal{J}(m_\pi,-\Delta,\mu)\right)\right]+Am_\pi^2. \tag{64}$$

The Δ field renormalization is

$$Z_\Delta = 1-\frac{1}{32\pi^2 f_\pi^2}\left[\frac{25}{18}g_{\Delta\Delta}^2\mathcal{L}(m_\pi,\mu)+2c_A^2\mathcal{J}(m_\pi,-\Delta,\mu)\right], \tag{65}$$

and the loop integrals from Ref. [41] evaluated at the scale $\mu = 1$ GeV are

$$\begin{aligned}
\mathcal{L}(m,\mu) &= m^2\log\left(\frac{m^2}{\mu^2}\right),\\
\mathcal{K}(m,\Delta,\mu) &= \left(m^2-\frac{2}{3}\Delta^2\right)\log\left(\frac{m^2}{\mu^2}\right)+\frac{2}{3}\Delta\sqrt{\Delta^2-m^2}\log\left(\frac{\Delta-\sqrt{\Delta^2-m^2+i\epsilon}}{\Delta+\sqrt{\Delta^2-m^2+i\epsilon}}\right)\\
&\quad+\frac{2}{3}\frac{m^2}{\Delta}\left(\pi m-\sqrt{\Delta^2-m^2}\log\left(\frac{\Delta-\sqrt{\Delta^2-m^2+i\epsilon}}{\Delta+\sqrt{\Delta^2-m^2+i\epsilon}}\right)\right),\\
\mathcal{J}(m,\Delta,\mu) &= (m^2-2\Delta^2)\log\left(\frac{m^2}{\mu^2}\right)+2\Delta\sqrt{\Delta^2-m^2}\log\left(\frac{\Delta-\sqrt{\Delta^2-m^2+i\epsilon}}{\Delta+\sqrt{\Delta^2-m^2+i\epsilon}}\right).
\end{aligned} \tag{66}$$

From the available lattice data on $C_5^A(q^2=0;m_\pi^2)$, $g_A(m_\pi^2)$, and $G_{\Delta\Delta}(m_\pi^2)$, we perform a simultaneous seven-parameter fit to expressions (60), (62), and (64), fitting the unknown constants a_1, a_2, A, $C^{\rm SSE}$ as well as the common chiral couplings g_A, c_A, and $g_{\Delta\Delta}$. We note that $C^{\rm SSE}$ is independent of m_π; at a fixed value of λ, it can be fitted as a constant.

The lattice nucleon axial charge values $g_A(m_\pi^2)$ are taken from twisted mass simulations [27]. Lattice values for the real part of the axial N-Δ couplings $C_5^A(0)$ are taken from Ref. [23] via a dipole extrapolation. The values of the real part of the axial charge of the Δ, $G_{\Delta\Delta}(m_\pi^2)$ are related to the dominant axial form factor g_1 at zero momentum transfer via $G_{\Delta\Delta}=-3g_1(0)$. For an additional lattice point to assist the fit, we computed the zero-momentum g_1 values (only) on the $20^3\times 64$ mixed-action ensemble with $m_\pi = 498$ MeV. Values are provided in Table X.

TABLE X. Numerical values for the dominant form factor $g_1(0)$ on each of the ensembles. $G_{\Delta\Delta}=-3g_1(0)$ with our normalization.

m_π (GeV)	$g_1(0)$
Quenched	
0.563(4)	0.589(10)
0.490(4)	0.578(13)
0.411(4)	0.571(18)
Mixed action	
0.498(3)	0.573(23)
0.353(2)	0.640(26)
DWF	
0.297(5)	0.604(38)

In Fig. 19 the combined fit is presented. The available lattice data for all three observables vary mildly in the pion mass regime considered. g_A remains underestimated with respect to the experimental value, and the inclusion of C_5^A and $G_{\Delta\Delta}$ into the SSE fit does not improve this systematically observed behavior. Strong chiral effects are expected at lighter pion mass values, especially below the Δ decay threshold, as is evident from the one-loop trend of C_5^A and $G_{\Delta\Delta}$.

VI. CONCLUSIONS

A detailed study of the axial structure of the $\Delta(1232)$ has been presented, complementing recent and ongoing studies of the axial structure of the nucleon as well as the axial N-to-Δ transition. The matrix element of the Δ state with the axial current has been parametrized via four Lorentz

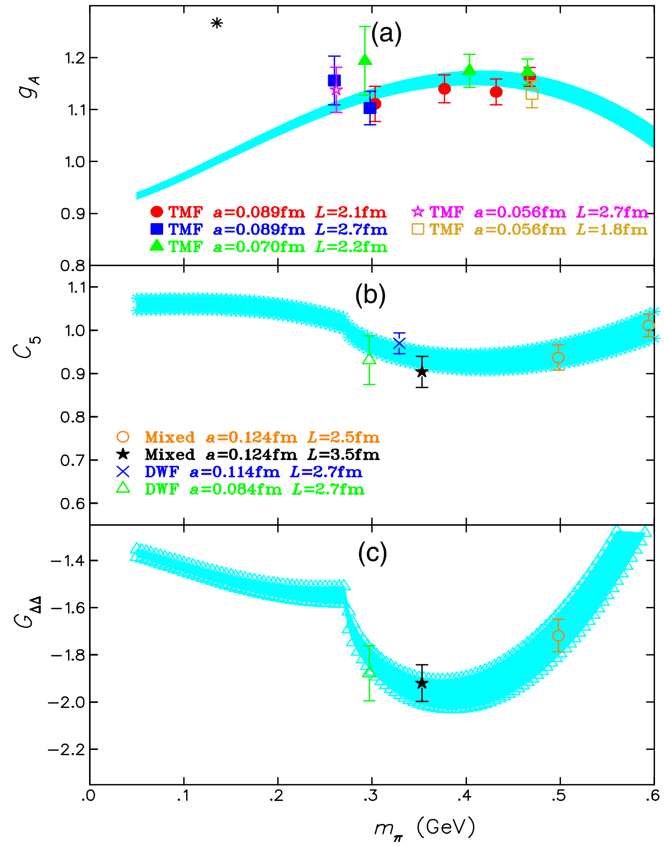

FIG. 19 (color online). Combined chiral fit: (a) Nucleon axial charge, g_A, fitted to lattice data obtained with $N_f = 2$ twisted mass fermions [27]. The physical value is shown by the asterisk (filled circles: $a = 0.089$ fm, $L = 2.1$; filled squares: $a = 0.089$ fm, $L = 2.8$ fm; filled triangles: $a = 0.070$ fm, $L = 2.2$ fm; open square: $a = 0.056$ fm, $L = 1.8$ fm; star: $a = 0.056$ fm, $L = 2.7$ fm); (b) real part of axial N-to-Δ transition coupling $C_5^A(0)$ [23] (open circles: $a = 0.124$ fm, $L = 2.5$ fm; filled square: $a = 0.124$ fm, $L = 3.5$ fm) and dynamical domain wall fermions (cross: $a = 0.114$ fm, $L = 2.7$ fm; open triangle: $a = 0.084$ fm, 2.7 fm); and (c) real part of Δ axial charge $G_{\Delta\Delta} = -3g_1(0)$.

invariant form factors, g_1, g_3, h_1, and h_3, a generalization of the familiar nucleon axial structure. Similarly, we parameterize the pseudoscalar matrix element with two form factors, denoted $\tilde{g}$ and $\tilde{h}$. We detailed the lattice techniques required for the extraction of all six form factors for a complete q^2-dependent evaluation via specially designed three-point functions. In fact, the calculation is optimized such that only two sequential propagators are needed for the numerical evaluation of the optimal correlators. The PCAC constrains strongly the nucleon matrix elements of the axial-vector and pseudoscalar currents as is manifestly evident by the phenomenological validity of the Goldberger-Treiman relation. Lattice QCD provides a check of this relation, which is a result of chiral symmetry breaking present in the QCD Lagrangian, confirming that the q^2 dependence of the axial and pseudoscalar form factors is in agreement with the PCAC predictions. Furthermore, the recent studies of the axial N-to-Δ transition have shown that the PCAC constrains strongly also the transition from factors and measurements of the dominant form factor C_5^A and $G_{\pi N\Delta}$ provided a check of the nondiagonal GT relation. This work examines extensions of similar relations for the Δ. The main result of the current work is that the PCAC plays a major role also in the relation between the Δ matrix elements of the axial-vector and pseudoscalar currents, connecting the strength of the π-Δ-Δ vertex to the Δ axial charge, $G_{\Delta\Delta}$. Actually, two independent pseudoscalar form factors, $G_{\pi\Delta\Delta}$ and $H_{\pi\Delta\Delta}$, are present, and pion-pole dominance establishes relations among all six form factors. These predictions are qualitatively verified using results obtained in the quenched QCD study, which carries the smallest statistical noise. Results from two dynamical ensembles are consistent with these findings, albeit within large statistical errors. Having obtained an evaluation of g_A and C_5^A from previous studies and using the results of this work for $G_{\Delta\Delta}$ on similar lattice ensembles, we performed a simultaneous chiral fit for all three using one-loop chiral effective theory predictions in the SSE scheme, which include a dynamical Δ field. The seven-parameter fit does not drive the prediction near the experimentally known g_A value, and this is not surprising as it has become recently clear that the correct value of g_A is not reproduced even with pion masses very close to the physical one. A careful isolation of excited state effects [42,43] at a pion mass of about 400 MeV failed to reveal excited-state contamination in the lattice extraction of g_A. Resolving such discrepancies is important for sharpening the predictive power of lattice QCD, which can yield phenomenologically important quantities not accessible experimentally. Fully chiral 2 + 1 domain wall flavor simulations are available now below the 300 MeV pion mass used in this work, and this leaves open the perspective for further investigations in the future, which will elaborate on the relations studied in this work and on the values of the major couplings that dominate the low-energy hadron interactions. However, as shown here, the gauge noise is large, and noise-reduction techniques will be needed in order to extract useful results using ensembles with close to physical pion masses.

ACKNOWLEDGMENTS

We are grateful to Brian Tiburzi and K. S. Choi for helpful discussions. E. B. G. was supported by Cyprus Research Promotion Foundation Grant No. ΔΙΕΘΝΗΣ/Σ ΤΟΧΟΣ/0308/07 and J. W. N. in part by funds provided by the U.S. Department of Energy (DOE) under cooperative research Agreement No. DE-FG02-94ER40818. Computer resources were provided by the National Energy Research Scientific Computing Center supported by the Office of Science of the DOE under Contract No. DE-AC02-05CH11231 and by the Jülich Supercomputing Center, awarded under the DEISA Extreme Computing Initiative, co-funded through the EU FP6 Project No. RI-031513 and the FP7 Project No. RI-222919. This research was in part supported by the Research Executive Agency of the European Union under Grant Agreement No. PITN-GA-2009-238353 (ITN STRONGnet) and the Cyprus Research Promotion Foundation under Contracts No. KY-ΓΑ/0310/02 and No. NEA ΥΠΟΔΟΜΗ/ΣΤΡΑΤΗ/0308/31 (infrastructure project Cy-Tera cofunded by the European Regional Development Fund and the Republic of Cyprus through the Research Promotion Foundation).

APPENDIX A: MULTIPOLE FORM FACTORS

The axial vector transition between Δ states can be parametrized via a multipole expansion. This is most naturally performed on the Breit frame, where $\vec{p}_f = -\vec{p}_i = \vec{q}/2$. Let us denote the matrix element as

$$\langle \Delta(\vec{q}/2, s_f)|\vec{A}\cdot\vec{\epsilon}_\lambda|\Delta(-\vec{q}/2, s_i)\rangle = M(s_f, s_i, \lambda). \quad \text{(A1)}$$

Generically four different transitions will occur parametrized via

$$\begin{aligned} M\left(\frac{1}{2},\frac{1}{2},0\right) &= L_1 + 3L_3 \\ M\left(\frac{3}{2},\frac{3}{2},0\right) &= 3L_1 - L_3 \\ M\left(\frac{1}{2},-\frac{1}{2},1\right) &= -2E_1 - \sqrt{6}E_3 \\ M\left(\frac{3}{2},\frac{1}{2},1\right) &= -\sqrt{3}E_1 + \sqrt{2}E_3, \end{aligned} \quad \text{(A2)}$$

with L_J, E_J the longitudinal and electric multipole amplitudes of rank J. The polarization vector $\vec{\epsilon}_\lambda$ has components $\vec{\epsilon}_+ = -(\hat{x} + i\hat{y})/\sqrt{2}$, $\vec{\epsilon}_- = -\vec{\epsilon}_+^*$, $\vec{\epsilon}_0 = \hat{z}$.

We can relate the form factors g_1, g_3, h_1, and h_3 to the multipole form factors E_1, E_3, L_1, and L_3, which have physical relevance in the multipole expansion,

$$\begin{aligned} g_1 &= \frac{3}{\sqrt{2}}E_1 + \sqrt{3}E_3 \\ \tau(1+\tau)h_1 &= -3\sqrt{2}\tau E_1 + \frac{5+4\tau}{2}\sqrt{3}E_3 \\ (g_1 - \tau g_3) &= \sqrt{1+\tau}(3L_1 - L_3) \\ \tau(1+\tau)(h_1 - \tau h_3) &= \sqrt{1+\tau}(-6\tau L_1 + (5+2\tau)L_3), \end{aligned} \quad \text{(A3)}$$

from which the reverse relations can be verified:

$$E_1 = \frac{\sqrt{2}g_1}{3} - \frac{2\sqrt{2}\tau(2g_1 + h_1(1+\tau))}{3(5+8\tau)} \quad \text{(A4)}$$

$$E_3 = \frac{2\tau(2g_1 + h_1(1+\tau))}{\sqrt{3}(5+8\tau)} \quad \text{(A5)}$$

$$L_1 = \frac{(5+2\tau)(g_1 - \tau g_3) + \tau(1+\tau)(h_1 - \tau h_3)}{15\sqrt{1+\tau}} \quad \text{(A6)}$$

$$L_3 = \tau\frac{2(g_1 - \tau g_3) + (1+\tau)(h_1 - \tau h_3)}{5\sqrt{1+\tau}}. \quad \text{(A7)}$$

Using the above relations, we present results on the four multipole axial form factors, E_1, E_3, L_1, and L_3, in Figs. 20–23, respectively.

In the low momentum transfer limit, $\tau \sim \mathcal{O}(\vec{q}^2/M_\Delta^2) \ll 1$, and from relations (A5) and (A7), we deduce that E_3, $L_3 \ll 1$. On the other hand, E_1 and L_1 remain finite, as from relation (A4) $E_1 \sim \sqrt{2}g_1/3$ and from (A6) $L_1 \sim g_1/3$. Thus, at the low momentum transfer limit, we expect that $E_1 = \sqrt{2}L_1 + \mathcal{O}(\vec{q}^2)$.

We test these predictions explicitly in Fig. 24, where the ratio $E_1/\sqrt{2}L_1$ is plotted. We observe a behavior consistent

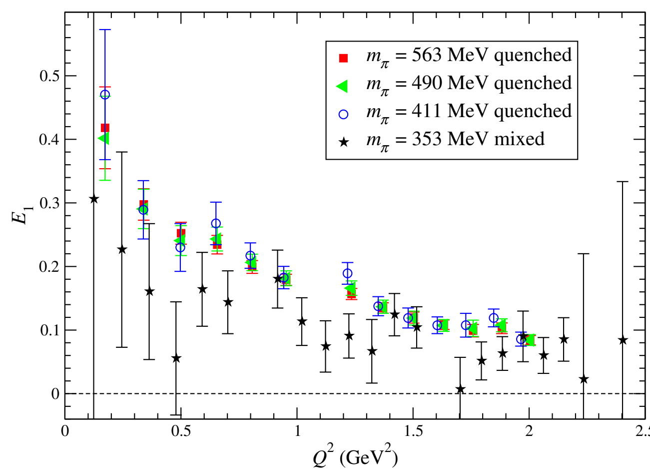

FIG. 20 (color online). Lattice results for the E_1 multipole axial form factor.

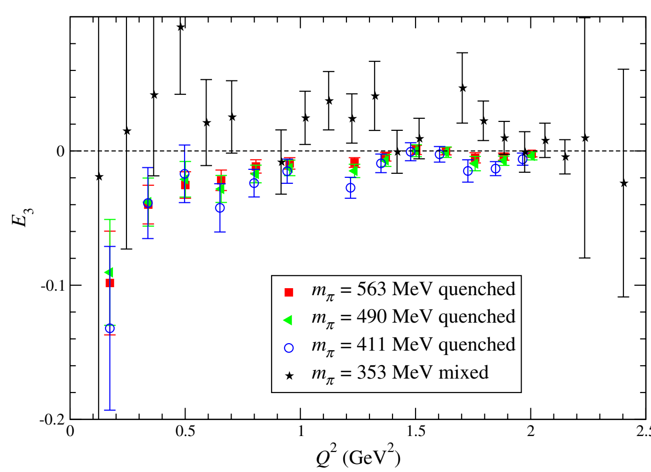

FIG. 21 (color online). Lattice results for the E_3 multipole axial form factor.

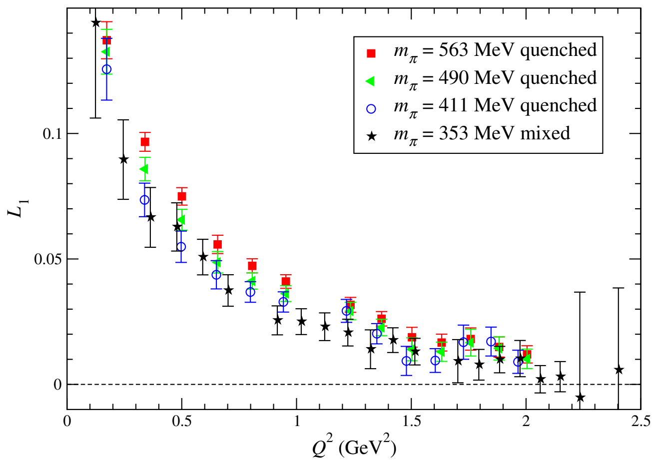

FIG. 22 (color online). Lattice results for the L_1 multipole axial form factor.

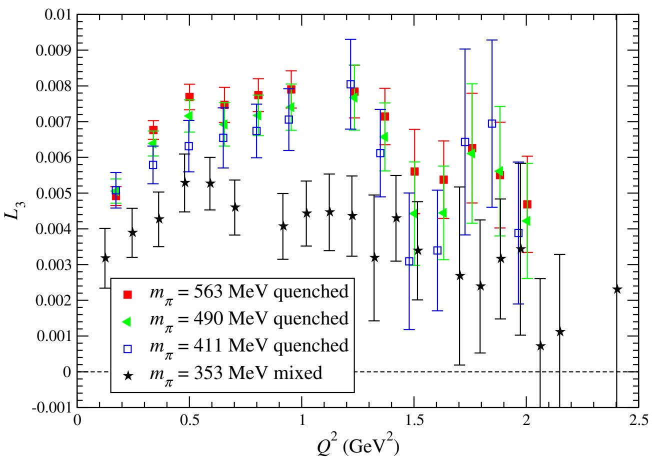

FIG. 23 (color online). Lattice results for the L_3 multipole axial form factor.

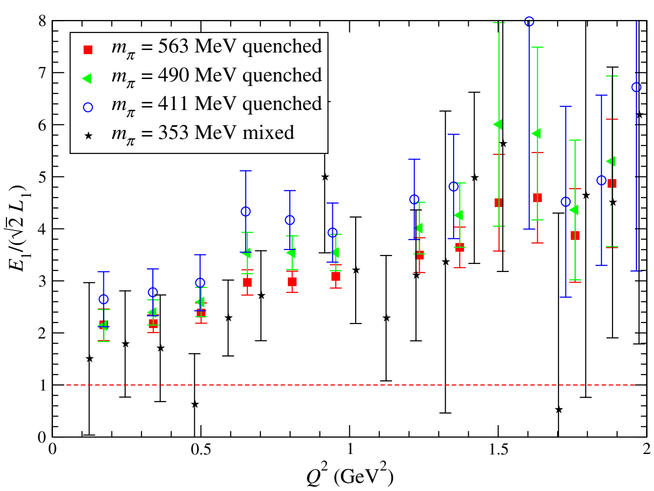

FIG. 24 (color online). Lattice results for the ratio of the E_1 to $\sqrt{2}L_1$ multipole axial form factors for the quenched ensembles.

with a constant in the low-energy (< 0.5 GeV^2) regime, although the numeric value of the constant is largely overestimated by the quenched lattice data. In addition, this constancy is in accordance to the pion-pole dependence of both E_1 and L_1, which is evident from the quenched lattice data plotted in Figs. 20 and 22. Despite the large statistical uncertainties, E_3 and L_3 are consistent with small values at small momentum transfers.

APPENDIX B: TRACE ALGEBRA FOR THREE-POINT CORRELATORS

1. Axial current correlator

We define type I as

$$\Pi^{IA}_{\mu}(q) \equiv \sum_{i=1}^{3}\sum_{\sigma,\tau=1}^{3}\delta_{\sigma\tau}\,\mathrm{tr}[\Gamma^i\Lambda_{\sigma\sigma'}(p_f)\mathcal{O}^A_{\sigma'\mu\tau'}\Lambda_{\tau'\tau}(p_i)]. \tag{B1}$$

After evaluating the Dirac traces, we find two distinct cases, $\mu = 4$ and $\mu = 1, 2, 3$. The kinematical frame is set to $\vec{p}_f = 0$ and $\vec{p}_i = -\vec{q}$. We note by $E = (\vec{p}^2 + M_\Delta^2)^{1/2}$.

For $\mu = 4$ we find

$$\begin{aligned}\Pi^{IA}_{\mu=4}(q) = \frac{-1}{36M_\Delta^3}&[2(2E^2 - 2EM_\Delta + 5M_\Delta^2)(g_1 - \tau g_3)\\ &- \tau(2E - M_\Delta)(E + M_\Delta)(h_1 - \tau h_3)]\\ &\times (p_1 + p_2 + p_3),\end{aligned} \tag{B2}$$

using

$$\tau \equiv \frac{(E - M_\Delta)}{2M_\Delta} = \frac{Q^2}{(2M_\Delta)^2}. \tag{B3}$$

For $\mu = i$ we find

$$\begin{aligned}\Pi^{IA}_{\mu=i}(q) = &\frac{i(E+M_\Delta)}{18M_\Delta^3}[(2E^2+3M_\Delta^2)g_1 - \tau E(E+M_\Delta)h_1]\\ &-\frac{i}{72M_\Delta^4}[8M_\Delta^2 g_1 + 2(2E^2 - 2EM_\Delta + 5M_\Delta^2)g_3\\ &- M_\Delta(E+M_\Delta)h_1 - \tau(E+M_\Delta)(2E - M_\Delta)h_3]\\ &\times p_i(p_1 + p_2 + p_3).\end{aligned} \tag{B4}$$

We define type II as

$$\Pi^{IIA}_{\mu}(q) \equiv \sum_{\sigma,\tau=1}^{3} T_{\sigma\tau}\,\mathrm{tr}[\Gamma^4\Lambda_{\sigma\sigma'}(p_f)\mathcal{O}^A_{\sigma'\mu\tau'}\Lambda_{\tau'\tau}(p_i)] \tag{B5}$$

$$T_{\sigma\tau} = \begin{bmatrix} 0 & 1 & -1 \\ -1 & 0 & 1 \\ 1 & -1 & 0 \end{bmatrix}. \tag{B6}$$

For $\mu = 4$ we find

$$\Pi^{II\mathrm{A}}_{\mu=4}(q) = \frac{i}{18M_\Delta^2}\Big[(E+4M_\Delta)(g_1-\tau g_3) - \frac{\tau}{2}(E+M_\Delta)(h_1-\tau h_3)\Big](p_1+p_2+p_3). \tag{B7}$$

For $\mu = i$ we find

$$\Pi^{II\mathrm{A}}_{\mu=i}(q) = \frac{(E+M_\Delta)^2}{36M_\Delta^3}[(2E+3M_\Delta)g_1 - \tau(E+M_\Delta)h_1] - \frac{1}{36M_\Delta^3}\Big[(2E+5M_\Delta)g_1 + (E+4M_\Delta)g_3 - \frac{E}{2m}(E+M_\Delta)h_1 - \frac{\tau}{2}(E+M_\Delta)h_3\Big] \times p_i(p_1+p_2+p_3). \tag{B8}$$

2. Pseudoscalar density correlator

In a similar way we evaluate the trace algebra for the pseudoscalar vertices. The index summation types are defined in the same way as in the axial case. Pseudoscalar type I is

$$\Pi^{I}_{\mathrm{PS}}(q) \equiv \sum_{i=1}^{3}\sum_{\sigma,\tau=1}^{3}\delta_{\sigma\tau}\,\mathrm{tr}[\Gamma^i\Lambda_{\sigma\sigma'}(p_f)\mathcal{O}^{\mathrm{PS}}_{\sigma'\tau'}\Lambda_{\tau'\tau}(p_i)]. \tag{B9}$$

After the trace evaluation, we find

$$\Pi^{I}_{\mathrm{PS}}(q) = \frac{-1}{18M_\Delta^3}\Big[\tilde{g}(2E^2-2EM_\Delta+5M_\Delta^2) - \tilde{h}\frac{\tau}{2}(2E-M_\Delta)(E+M_\Delta)\Big](p_1+p_2+p_3) \tag{B10}$$

Pseudoscalar type II is

$$\Pi^{II}_{\mathrm{PS}}(q) \equiv \sum_{\sigma,\tau=1}^{3} T_{\sigma\tau}\,\mathrm{tr}[\Gamma^4\Lambda_{\sigma\sigma'}(p_f)\mathcal{O}^{\mathrm{PS}}_{\sigma'\tau'}\Lambda_{\tau'\tau}(p_i)], \tag{B11}$$

giving us

$$\Pi^{II}_{\mathrm{PS}}(q) = \frac{i}{18M_\Delta^2}\Big[(E+4M_\Delta)\tilde{g} - \frac{\tau}{2}(E+M_\Delta)\tilde{h}\Big] \times (p_1+p_2+p_3) \tag{B12}$$

after we evaluate the trace.

APPENDIX C: FORM FACTOR RESULTS

TABLE XI. Delta form factors from quenched Wilson fermions.

		Axial				Pseudoscalar	
	Q^2 (GeV^2)	g_1	g_3	h_1	h_3	$\tilde{g}$	$\tilde{h}$
	0.000000	0.5887(98)	...	...	...	...	...
	0.1730731	0.717(70)	15.3(3.2)	22.9(8.6)	740(380)	9.58(43)	46(89)
	0.3396915	0.562(27)	6.96(65)	5.6(1.7)	103(37)	7.14(19)	46(17)
	0.5005274	0.491(20)	4.63(38)	2.89(79)	38(16)	5.42(18)	17.4(8.5)
	0.6561444	0.459(19)	3.86(25)	2.15(48)	24.7(7.4)	4.13(17)	10.3(5.5)
	0.8070197	0.403(14)	2.81(15)	1.30(26)	11.7(3.1)	3.44(14)	10.1(2.9)
	0.9535618	0.364(14)	2.20(11)	1.04(19)	7.7(2.1)	2.91(13)	8.6(1.9)
	1.235014	0.318(14)	1.57(10)	0.84(14)	4.4(1.1)	2.12(14)	5.5(1.3)
$m_\pi = 563(4)$ MeV	1.370502	0.279(14)	1.272(81)	0.61(11)	2.91(87)	1.73(12)	4.21(92)
	1.502826	0.255(14)	1.151(89)	0.41(11)	2.38(79)	1.35(13)	2.34(90)
	1.632198	0.230(13)	0.959(68)	0.388(84)	1.97(54)	1.17(11)	2.08(69)
	1.758807	0.201(17)	0.730(86)	0.45(11)	1.84(64)	1.05(14)	1.95(72)
	1.882824	0.211(16)	0.769(76)	0.439(69)	1.69(41)	0.92(13)	1.52(57)
	2.004400	0.175(14)	0.604(65)	0.327(58)	1.24(31)	0.73(10)	1.18(43)
	2.240774	0.124(22)	0.43(11)	3.249(98)	4.66(48)	0.40(16)	0.48(60)

TABLE XII. Delta form factors from quenched Wilson fermions.

		Axial				Pseudoscalar	
	Q^2 (GeV^2)	g_1	g_3	h_1	h_3	$\tilde{g}$	$\tilde{h}$
$m_\pi = 490(4)$ MeV	0.000000	0.578(13)	...	...	...	...	...
	0.1728690	0.695(72)	14.0(2.9)	20.0(8.3)	390(330)	10.85(62)	120(130)
	0.3389351	0.550(36)	7.03(78)	5.1(2.0)	97(41)	7.69(27)	59(23)
	0.4989433	0.474(28)	4.52(45)	2.4(1.1)	33(17)	5.78(23)	26(11)
	0.6535119	0.467(23)	3.99(31)	2.45(60)	26.8(9.0)	4.23(22)	10.3(6.8)
	0.8031605	0.408(17)	2.88(18)	1.53(33)	13.1(3.6)	3.54(17)	11.6(3.3)
	0.9483310	0.363(16)	2.18(14)	1.14(25)	8.1(2.4)	2.98(16)	8.9(2.3)
	1.226705	0.326(17)	1.58(12)	1.02(18)	5.1(1.4)	2.21(17)	5.9(1.5)
	1.360524	0.278(16)	1.253(95)	0.67(14)	3.2(1.0)	1.75(14)	4.1(1.1)
	1.491113	0.252(17)	1.14(10)	0.42(13)	2.59(93)	1.30(14)	2.0(1.1)
	1.618694	0.226(15)	0.935(78)	0.40(11)	2.02(63)	1.15(13)	2.01(82)
	1.743467	0.202(20)	0.71(10)	0.54(14)	2.17(77)	1.02(16)	1.50(89)
	1.865609	0.216(19)	0.751(87)	0.501(87)	1.74(48)	0.99(15)	1.79(70)
	1.985279	0.173(16)	0.580(71)	0.348(73)	1.25(36)	0.73(12)	1.10(50)
	2.217769	0.110(24)	0.41(12)	−0.09(13)	−0.02(58)	0.31(18)	0.21(72)

TABLE XIII. Delta form factors from quenched Wilson fermions. Results for h_1 and h_3 are plagued by statistical noise.

		Axial				Pseudoscalar	
	Q^2 (GeV^2)	g_1	g_3	h_1	h_3	$\tilde{g}$	$\tilde{h}$
$m_\pi = 411(4)$ MeV	0.000000	0.571(18)	...	...	...	...	...
	0.1726468	0.77(11)	17.4(4.5)	27(12)	560(490)	13.1(1.1)	290(230)
	0.3381149	0.546(52)	7.4(1.1)	4.9(2.7)	102(61)	8.27(45)	59(40)
	0.4972318	0.458(44)	4.53(66)	2.0(1.6)	33(24)	6.17(36)	27(18)
	0.6506769	0.495(41)	4.28(51)	3.2(1.0)	32(15)	4.48(31)	15.4(9.8)
	0.7990168	0.419(26)	2.96(25)	1.81(49)	13.4(5.2)	3.73(23)	14.4(4.4)
	0.9427295	0.361(23)	2.14(19)	1.21(37)	7.5(3.4)	3.16(22)	11.2(3.2)
	1.217848	0.354(25)	1.68(16)	1.42(26)	6.4(2.0)	2.41(25)	7.5(2.3)
	1.349909	0.276(22)	1.23(12)	0.72(21)	3.4(1.4)	1.78(18)	4.4(1.4)
	1.478675	0.251(24)	1.16(13)	0.44(19)	3.1(1.3)	1.23(18)	1.8(1.5)
	1.604379	0.224(20)	0.93(10)	0.43(16)	2.26(87)	1.15(16)	2.4(1.1)
	1.727230	0.203(28)	0.68(13)	0.65(21)	2.5(1.1)	0.96(21)	1.0(1.3)
	1.847415	0.230(24)	0.75(11)	0.63(13)	1.87(64)	1.16(20)	2.9(1.0)
	1.965099	0.171(18)	0.565(85)	0.39(10)	1.32(47)	0.73(15)	1.13(68)
	2.193551	9.100(30)	0.37(14)	−0.18(19)	8.70(83)	0.16(21)	−0.2(1.1)

TABLE XIV. Delta form factors from mixed-action fermions.

		Axial				Pseudoscalar	
	Q^2 (GeV^2)	g_1	g_3	h_1	h_3	$\tilde{g}$	$\tilde{h}$
	0.000000	0.640(26)	...	...	...	...	...
	0.1240682	0.62(39)	15(26)	8(74)	−100(4500)	14.4(4.8)	230(1800)
	0.2450231	0.51(17)	9.8(6.0)	−2(16)	120(540)	11.7(1.8)	440(320)
	0.3630880	0.41(12)	6.0(3.1)	−4.4(7.7)	−25(200)	9.1(1.2)	260(140)
	0.4784607	0.28(10)	1.9(2.1)	−8.1(4.9)	−160(104)	7.0(1.1)	87(83)
	0.5913172	0.385(69)	4.0(1.1)	−0.9(2.5)	−7(40)	5.88(67)	85(37)
	0.7018154	0.349(60)	3.42(78)	−1.0(1.9)	2(25)	5.41(61)	87(27)
	0.9162911	0.368(57)	3.22(60)	1.1(1.3)	21(15)	3.46(56)	29(17)
	1.020513	0.283(47)	2.07(43)	−0.6(1.0)	−0.3(9.3)	3.43(51)	35(12)
	1.122869	0.222(50)	1.39(43)	−1.15(98)	−9.6(8.5)	2.22(52)	17(11)
	1.223456	0.234(45)	1.43(36)	−0.50(77)	−3.2(6.3)	2.26(48)	13.3(8.5)
$m_\pi = 353(4)$ MeV	1.322363	0.212(66)	1.31(51)	−1.1(1.0)	−5.6(8.1)	2.34(77)	18(13)
	1.419670	0.262(46)	1.50(31)	0.48(60)	2.5(4.2)	1.70(50)	7.0(7.1)
	1.515454	0.237(48)	1.32(30)	0.12(53)	2.0(3.6)	2.08(54)	12.3(6.3)
	1.702723	9.586(67)	0.41(38)	−1.15(83)	−6.4(4.8)	1.25(99)	14(11)
	1.794332	0.148(44)	0.70(24)	−0.35(44)	−1.8(2.5)	1.07(56)	8.4(5.2)
	1.884666	0.151(39)	0.65(20)	0.00(66)	−0.3(2.0)	0.90(48)	3.1(4.0)
	1.973777	0.190(66)	0.82(32)	0.34(44)	1.3(2.3)	0.65(67)	−6.1(5.8)
	2.061714	0.141(42)	0.66(20)	0.05(35)	0.5(1.8)	0.37(52)	5.4(4.0)
	2.148521	0.173(56)	0.77(26)	0.38(35)	2.1(1.7)	1.07(59)	4.3(4.1)
	2.234241	0.06(31)	0.4(1.6)	−0.1(2.6)	0.0(11.0)	−0.5(3.5)	−5(32)
	2.402577	0.14(39)	0.5(1.5)	0.7(2.3)	2.5(9.2)	1.0(3.4)	2(18)

TABLE XV. Delta form factors from domain wall fermions.

		Axial				Pseudoscalar	
	Q^2 (GeV^2)	g_1	g_3	h_1	h_3	$\tilde{g}$	$\tilde{h}$
	0.0	0.604(38)	...	...	...	...	...
	0.2060893	0.08(45)	−5.6(18.0)	−44(45)	−1500(2000)	9.4(9.3)	−1100(1800)
	0.4030337	0.66(20)	9.3(4.3)	11(10)	130(240)	6.6(3.0)	−300(280)
	0.5919523	0.79(19)	10.3(2.9)	13(6)	210(110)	4.5(2.4)	−82(140)
	0.7737530	0.41(20)	3.5(2.3)	2.2(5.2)	8(65)	7.2(2.2)	125(90)
	0.9491845	0.21(12)	0.6(1.7)	−1.0(2.5)	−34(25)	4.5(1.3)	42(39)
	1.118873	0.51(14)	3.9(1.1)	4.8(2.2)	45(19)	1.3(1.4)	−20(32)
	1.443061	0.47(21)	2.3(1.3)	4.3(2.6)	21(17)	3.2(1.9)	27(30)
	1.598405	0.31(14)	1.25(76)	2.1(1.6)	4.7(8.8)	0.1(1.2)	−1(16)
	1.749719	0.14(13)	0.91(69)	0.0(1.3)	2.2(7.2)	0.2(1.4)	−12(16)
	1.897302	−0.09(29)	−0.3(1.4)	−2.2(3.2)	−11(16)	−4.6(4.6)	−62(57)
$m_\pi = 297(5)$ MeV	2.041417	−0.03(33)	0.1(1.6)	−0.4(2.9)	3(14)	0.2(3.1)	6(33)
	2.182297	0.17(23)	0.51(91)	0.8(1.8)	4.6(7.7)	2.8(2.7)	9(18)
	2.320150	−0.06(14)	−0.41(57)	−0.7(1.1)	−3.6(4.4)	0.4(1.4)	2(11)

[1] K. Jansen, Proc. Sci., LATTICE2008 (2008) 010 [arXiv:0810.5634].
[2] S. Durr *et al.*, Science **322**, 1224 (2008).
[3] S. Aoki *et al.* (PACS-CS), Phys. Rev. D **79**, 034503 (2009).
[4] S. Durr, Z. Fodor, C. Hoelbling, S. D. Katz, S. Krieg, T. Kurth, L. Lellouch, T. Lippert, K. K. Szabó, and G. Vulvert, J. High Energy Phys. 08 (2011) 148.
[5] C. Alexandrou, R. Baron, J. Carbonell, V. Drach, P. Guichon, K. Jansen, T. Korzec, and O. Pène (ETM Collaboration), Phys. Rev. D **80**, 114503 (2009).
[6] S. Aoki *et al.* (PACS-CS Collaboration), Phys. Rev. D **81**, 074503 (2010).
[7] S. R. Beane, E. Chang, W. Detmold, H. W. Lin, T. C. Luu, K. Orginos, A. Parreño, M. J. Savage, A. Torok, and A. Walker-Loud (NPLQCD Collaboration), Phys. Rev. D **85**, 034505 (2012).
[8] J. J. Dudek, R. G. Edwards, and C. E. Thomas, Phys. Rev. D **86**, 034031 (2012).
[9] X. Feng, K. Jansen, and D. B. Renner, Phys. Lett. B **684**, 268 (2010).
[10] T. Yamazaki *et al.* (*CP*-PACS Collaboration), Phys. Rev. D **70**, 074513 (2004).
[11] M. Kotulla, J. Ahrens, J. Annand, R. Beck, G. Caselotti *et al.*, Phys. Rev. Lett. **89**, 272001 (2002).
[12] G. Lopez Castro and A. Mariano, Phys. Lett. B **517**, 339 (2001).
[13] V. Bernard, T. R. Hemmert, and U.-G. Meissner, Phys. Lett. B **622**, 141 (2005).
[14] T. R. Hemmert, B. R. Holstein, and J. Kambor, J. Phys. G **24**, 1831 (1998).
[15] E. E. Jenkins and A. V. Manohar, Phys. Lett. B **259**, 353 (1991).
[16] N. Fettes and U. G. Meissner, Nucl. Phys. **A679**, 629 (2001).
[17] T. R. Hemmert, M. Procura, and W. Weise, Phys. Rev. D **68**, 075009 (2003).
[18] V. Bernard, Prog. Part. Nucl. Phys. **60**, 82 (2008).
[19] R. F. Dashen, E. E. Jenkins, and A. V. Manohar, Phys. Rev. D **49**, 4713 (1994).
[20] G. Brown and W. Weise, Phys. Rep. **22**, 279 (1975).
[21] K.-S. Choi, W. Plessas, and R. Wagenbrunn, Phys. Rev. D **82**, 014007 (2010).
[22] C. Alexandrou, G. Koutsou, T. Leontiou, J. W. Negele, and A. Tsapalis, Phys. Rev. D **76**, 094511 (2007).
[23] C. Alexandrou, G. Koutsou, J. Negele, Y. Proestos, and A. Tsapalis, Phys. Rev. D **83**, 014501 (2011).
[24] C. Alexandrou, T. Korzec, G. Koutsou, C. Lorce, J. W. Negele, V. Pascalutsa, A. Tsapalis, and M. Vanderhaeghen, Nucl. Phys. **A825**, 115 (2009).
[25] C. Alexandrou, C. Papanicolas, and M. Vanderhaeghen, Rev. Mod. Phys. **84**, 1231 (2012).
[26] C. Alexandrou, E. B. Gregory, T. Korzec, G. Koutsou, J. W. Negele, T. Sato, and A. Tsapalis, Phys. Rev. Lett. **107**, 141601 (2011).
[27] C. Alexandrou, M. Brinet, J. Carbonell, M. Constantinou, P. A. Harraud, P. Guichon, K. Jansen, T. Korzec, and M. Papinutto (ETM Collaboration), Phys. Rev. D **83**, 045010 (2011).
[28] F.-J. Jiang and B. C. Tiburzi, Phys. Rev. D **78**, 017504 (2008).
[29] J. A. M. Vermaseren, arXiv:math-ph/0010025.
[30] A. Tsapalis, Nucl. Phys. B, Proc. Suppl. **153**, 320 (2006).
[31] C. W. Bernard, T. Burch, K. Orginos, D. Toussaint, T. A. DeGrand, C. DeTar, S. Datta, S. Gottlieb, U. Heller, and R. Sugar, Phys. Rev. D **64**, 054506 (2001).
[32] M. Albanese *et al.* (APE Collaboration), Phys. Lett. B **192**, 163 (1987).
[33] Y. Aoki *et al.* (RBC Collaboration, UKQCD Collaboration), Phys. Rev. D **83**, 074508 (2011).
[34] V. M. Belyaev, B. Y. Blok, and Y. I. Kogan, Sov. J. Nucl. Phys. **41**, 280 (1985).
[35] S.-L. Zhu, Phys. Rev. C **63**, 018201 (2000).
[36] G. Erkol, http://irs.ub.rug.nl/ppn/297396218.
[37] D. Jido, T. Hatsuda, and T. Kunihiro, Phys. Rev. Lett. **84**, 3252 (2000).
[38] A. C. Cordon and J. Goity, arXiv:1303.2126.
[39] M. Procura, Phys. Rev. D **78**, 094021 (2008).
[40] M. Procura, B. Musch, T. Hemmert, and W. Weise, Phys. Rev. D **75**, 014503 (2007).
[41] F.-J. Jiang and B. C. Tiburzi, Phys. Rev. D **77**, 094506 (2008).
[42] S. Dinter, C. Alexandrou, M. Constantinou, V. Drach, K. Jansen, and D. B. Renner, Phys. Lett. B **704**, 89 (2011).
[43] C. Alexandrou, M. Constantinou, S. Dinter, V. Drach, K. Jansen *et al.*, Proc. Sci., LATTICE2011 (2011) 150.